RESEARCH ARTICLE

An actin–myosin-II interaction is involved in maintaining the contractile ring in fission yeast

Masak Takaine*,‡, Osamu Numata and Kentaro Nakano‡

ABSTRACT

The actomyosin-based contractile ring, which assembles at the cell equator, maintains its circularity during cytokinesis in many eukaryotic cells, ensuring its efficient constriction. Although consistent maintenance of the ring is one of the mechanisms underpinning cytokinesis, it has not yet been fully addressed. We here investigated the roles of fission yeast myosin-II proteins [Myo2 and Myo3 (also known as Myp2)] in ring maintenance during cytokinesis, with a focus on Myo3. A site-directed mutational analysis showed that the motor properties of Myo3 were involved in its accumulation in the contractile ring. The assembled ring was often deformed and not properly maintained under conditions in which the activities of myosin-II proteins localizing to the contractile ring were decreased, leading to inefficient cell division. Moreover, Myo3 appeared to form motile clusters on the ring. We propose that large assemblies of myosin-II proteins consolidate the contractile ring by continuously binding to F-actin in the ring, thereby contributing to its maintenance.

KEY WORDS: Cytokinesis, Contractile ring, Fission yeast, Myosin-II, Actin cytoskeleton

INTRODUCTION

After the completion of mitosis, one cell mechanically divides into two daughters, and this process is called cytokinesis. This coordinated cytofission ensures proper segregation of the genome and organelles, and its failure can induce changes in ploidy and oncogenesis or cell death (Ganem et al., 2007). Actin filaments (F-actin) and myosin-II both assemble into a circular structure along the cell equator, called the contractile ring, during cytokinesis in many eukaryotic cells. In addition to large amounts of F-actin and myosin-II, the contractile ring comprises various regulatory proteins such as actin-modulating proteins and signaling molecules, indicating the elaborate coordination of molecular systems (Eggert et al., 2006; Goyal et al., 2011). Similar to during the contraction of muscle sarcomeres, bipolar myosin-II filaments are considered to slide oppositely orientated F-actin filaments closer together in order to drive shrinkage of the contractile ring, which, in turn, generates the inwards force required for cortical ingression during cytokinesis (Wang, 2005; Pollard, 2010). This is called the purse-string model and is consistent with previous findings showing that contractile ring F-actin had mixed polarities (Sanger and Sanger, 1980; Maupin and Pollard, 1986; Kamasaki et al., 2007). The number of

sarcomere-like contractile units in the unconstricted contractile ring of *Caenorhabditis elegans* embryos has been suggested to reflect the scalability of the ring constriction rate: larger rings constrict faster than smaller ones (Carvalho et al., 2009).

Although a previous study has suggested that the motor activity of myosin-II is involved in the constriction of the contractile ring or cytokinesis (Straight et al., 2003), the precise configuration of actin and myosin-II in the ring and the mechanism by which the local actin–myosin interaction is harnessed for global shrinkage have yet to be elucidated. The motor activity of myosin-II has also been shown to promote the turnover of cortical actin during cytokinesis (Guha et al., 2005; Murthy and Wadsworth, 2005), which suggests that it functions in actin disassembly. Myosin-II has previously been shown to induce the disintegration of F-actin bundles *in vitro* and has been implicated in cellular actin network disassembly (Haviv et al., 2008; Wilson et al., 2010). Moreover, motor-impaired mutant myosin-II proteins have been shown to effectively support cytokinesis (Reichl et al., 2008; Ma et al., 2012), suggesting that myosin-II modulates cortical tension by crosslinking F-actin rather than sliding F-actin in the contractile ring during cytokinesis.

Two myosin-II isoforms in *Schizosaccharomyces pombe*, Myo2 and Myo3 (also called Myp2), both localize to the contractile ring and have been implicated in cytokinesis. Myo2 is essential for cell proliferation, whereas the function of Myo3 is vital for growth under certain conditions. During metaphase, the anillin-related protein Mid1 recruits Myo2 to the medial cortex as a broad band of nodes in an F-actin-independent manner, possibly through an interaction with the C-terminal tail moiety of Myo2 (Motegi et al., 2004). The motor activity of Myo2 has been suggested to drive the capture and pulling of F-actin elongated from the nodes, leading to the coalescence of these nodes and F-actin into a ring (Vavylonis et al., 2008), which indicates the primary role of Myo2 is in ring assembly. Myo3 is a single-headed myosin-II with a large gap in the coiled-coil region (Fig. 1A) and localizes to the ring in an F-actin-dependent manner (Wu et al., 2003). A double mutation of *myo3*Δ (a null mutation in *myo3*) and the *myo2-E1* (a temperature-sensitive allele of *myo2*; Balasubramanian et al., 1998) have previously been shown to cause severe defects in cytokinesis (Motegi et al., 2000). The motor heads of Myo2 and Myo3 are assumed to have similar properties because they have been found to be functionally exchangeable (Bezanilla and Pollard, 2000). Thus, although the two myosin-II proteins have been suggested to play an overlapping role, possibly through their head moieties, the underlying mechanism currently remains unclear. As Myo3 is single-headed, it is currently unclear whether and how it might be involved in contractile ring constriction, whereas Myo2 might assemble into bipolar filaments and contribute to ring constriction through the purse-string mechanism. In addition, previous studies have indicated that Myo3 is necessary for cell division in high-Cl⁻ environments. The molecular bases of the Cl⁻ tolerance of Myo3 and its relationship to the shared function with Myo2 also have not yet been elucidated.

Department of Biological Sciences, Graduate School of Life and Environmental Sciences, University of Tsukuba, 1-1-1 Tennohdai, Tsukuba, Ibaraki 305-8577, Japan.
*Present address: Gunma University Initiative for Advanced Research (GIAR), Gunma University, 3-39-15 Showa-machi, Maebashi, Gunma 371-8512, Japan.

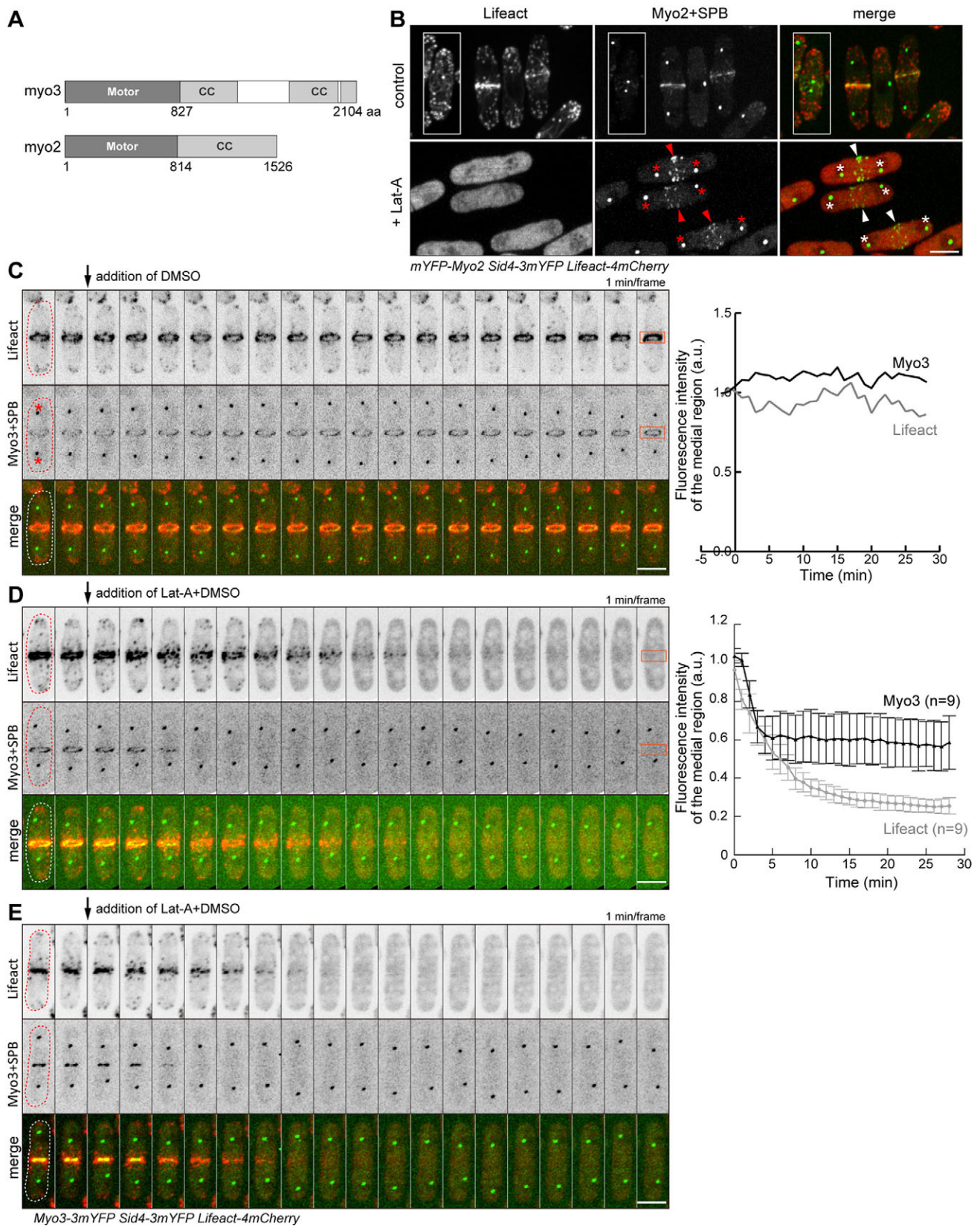‡Authors for correspondence (masaktakaine@gmail.com; knakano@biol.tsukuba.ac.jp)

Fig. 1. Localization of Myo3 to the contractile ring depends on F-actin throughout cytokinesis. (A) Structures of Myo3 and Myo2. CC, coiled-coil region. (B) Cells treated with 0.25% DMSO plus 0 or 8 µM Lat-A for 20 min. Arrowheads indicate some of the F-actin-independent cortical dots of mYFP–Myo2. Insets show a cell bearing the medial node mYFP–Myo2 structures. (C–E) Time-lapse imaging of Myo3–3mYFP rings. Myo3, Lifeact and SPBs in late anaphase cells were simultaneously imaged at 1-min intervals. DMSO (0.36%) alone (C) or DMSO plus 7 µM Lat-A (D) was supplemented at the indicated time-points. Right, mean fluorescence intensities of the boxed regions plotted over time. Data in D are the mean±s.d., and pooled from two independent experiments. (E) Cells having constricting rings were similarly treated with Lat-A. Asterisks indicate some SPBs for clarity. Scale bars: 5 µm.

In the present study, we focused on Myo3 in order to examine the role of myosin-II following contractile ring assembly. Myo3 localized to the contractile ring following the assembly of the actin ring, in a manner that was solely dependent on F-actin. A site-directed mutational analysis revealed that the motor properties of Myo3 were required for its localization to the medial region. Under conditions in which the local accumulation of Myo3 and motor activity of Myo2 were both reduced, the contractile ring that assembled was not maintained properly in a proportion of cells, resulting in inefficient septation, which suggests that myosin-II proteins have a collaborative role in maintaining the ring. Moreover, Myo3 appeared to form motile clusters on the ring. We propose that large assemblies, bipolar filaments or clusters of myosin-II proteins consolidate the contractile ring by continuously binding to F-actin in the ring, thereby cooperatively contributing to its maintenance during cytokinesis.

RESULTS
Myo3 localizes to the contractile ring by solely depending on actin filaments

We recently reported that several components of the contractile ring of the fission yeast *S. pombe*, including Myo2, can localize to this structure through both F-actin-dependent and -independent mechanisms, even after the completion of ring assembly, such that when F-actin is lost a fraction of the component remains at the cortical ring (Takaine et al., 2014a). Consistent with our previous findings, we found that mYFP–Myo2 colocalized with F-actin in the medial region as a node structure at early anaphase and as a ring at late anaphase (Fig. 1B). The localization of Lifeact was homogenous in cells treated with latrunculin-A (Lat-A), indicating that this drug causes the disassembly of cellular F-actin structures into undetectable actin subunits. Upon Lat-A treatment, Myo2 localized as medial cortical dots that could be distinguished from precursor nodes (Fig. 1B, arrowheads). We then attempted to determine whether another myosin-II, Myo3, in the contractile ring could also localize in both an F-actin-dependent and -independent manner. The Lat-A-induced dispersal of F-actin and localization of Myo3 were examined by time-lapse imaging. Myo3 and actin colocalized in the contractile ring at late anaphase. The exposure of cells to a low concentration of DMSO did not affect maintenance or constriction of the ring (Fig. 1C; supplementary material Movie 1). The addition of Lat-A disintegrated the actin–Myo3 ring and other F-actin structures within several minutes, suggesting that Myo3 localization to the ring was completely dependent on F-actin (Fig. 1D; supplementary material Movie 2). The decrease in fluorescence intensity in these rings favorably fitted a single exponential function. The half-decline time of Myo3 was slightly smaller than that of actin (1.6 versus 3.5 min; *P*=0.001). The disassembly of F-actin in the constricting ring similarly caused dispersion of the Myo3 signal (Fig. 1E). These results suggest that contractile ring F-actin is the primary and essential scaffold for Myo3 throughout cytokinesis.

Myo3 gradually accumulates on F-actin in the contractile ring

We simultaneously examined the accumulation kinetics of Myo3 and actin to the equatorial ring. In early anaphase, actin gradually accumulated at the cell middle, forming a thin ring (Fig. 2A; supplementary material Movie 3). As the actin ring thickened at late anaphase, the Myo3 signal began to increase in the medial region (Fig. 2B,C). The actin and Myo3 rings remained together in place for several minutes (known as the 'dwell time' of the ring), and then constricted in a synchronized manner. Myo3 localized only very

slightly to the F-actin net that is the precursor of the actin ring (Fig. 2D). Deconvolution microscopy revealed that the actin rings were almost continuous, suggesting that the concentration of actin in the contractile ring was constant, whereas the Myo3 rings were more inhomogeneous and discontinuous (Fig. 2E). Hence, Myo3 might preferentially localize to a limited number of sites on the actin ring. We further examined the formation of Myo3 and actin rings in *mid1Δ* cells, in which the contractile ring is assembled from strands, not from medial nodes (Saha and Pollard, 2012). In these cells, actin appeared as strands and assembled into a ring, and Myo3 formed a ring after the actin ring assembled (Fig. 2F,G). Thus, Myo3 might specifically interact with F-actin, which assembles into a ring that was nearly fully formed independently of Mid1.

Mutations in the motor moiety altered the local concentration of Myo3

The F-actin-dependent localization of Myo3 to the contractile ring implies that Myo3 interacts with F-actin in the ring through its motor domain. In order to investigate the relationship between the motor properties of Myo3 and its localization, we introduced several well-characterized point mutations into the highly conserved regions in the head moiety (Fig. 3A,B; supplementary material Fig. S1), which took advantage of *myo3* not being required for viability, in contrast to *myo2*. An immunoblot analysis demonstrated that these mutants were produced at the same level as wild-type (wt) (Fig. 3C). The E480K mutant corresponds to one of the mutant myosins that shows no detectable ATPase activity and actin filament sliding (Ruppel and Spudich, 1996). Myo3-E480K–3mYFP, which was expected to have no ATPase activity, showed no ring localization at anaphase (Fig. 3D). The R240A mutant Myo3 is predicted to have low-actin-activated ATPase activity and to not be able to drive F-actin sliding given that the original mutant myosin-II had a V_{max} value one-fifth that of wt, a K_m value 2.5-fold higher than that of wt, and also showed no motility (Shimada et al., 1997). Although Myo3-R240A localized to the contractile ring, its local concentration was 15% that of wt (Fig. 3D,E). The S469V mutant corresponds to a mutant myosin that retains high-actin-activated ATPase activity, but translocates F-actin at only one-tenth the speed of wt (indicating the uncoupling of ATPase activity and motility) (Ruppel and Spudich, 1996; Endow, 2000). The local concentration of Myo3-S469V in the contractile ring was approximately half that of wt (Fig. 3D,E). The R702C and R709C mutants of human non-muscle myosin IIA and myosin IIB show ~20% of the maximum actin-activated ATPase activity of wt and have a higher affinity for actin in the presence of ATP (its K_m value is less than one-third that of wt) owing to the very slow release of ADP (Kim et al., 2005). Moreover, the motilities of the mutant myosins are severely impaired (Hu et al., 2002; Kim et al., 2005). The local concentration of the corresponding Myo3-R694C mutant in the ring was 1.8-fold higher than that of wt (Fig. 3D,E). The G680V mutant myosin-II of *Dictyostelium discoideum* strongly binds to actin even in the presence of ATP by possibly forming a stable actin–myosin-II complex carrying ADP and phosphate (Patterson et al., 1997; Uyeda et al., 2002). The bulk of the corresponding Myo3-G688V mutant formed an aggregate in the medial region, whereas the rest localized faintly to the contractile ring (Fig. 3D). The aggregates were distinct from spindle pole bodies (SPBs) and often persisted during interphase (Fig. 3F). These results suggest that (1) an undisturbed ATP hydrolysis cycle is required for the proper distribution of Myo3 over the ring, and (2) that the Myo3 affinity for F-actin in the presence of ATP is relevant to its local concentration. The motility of Myo3 itself does not appear to be essential for its localization.
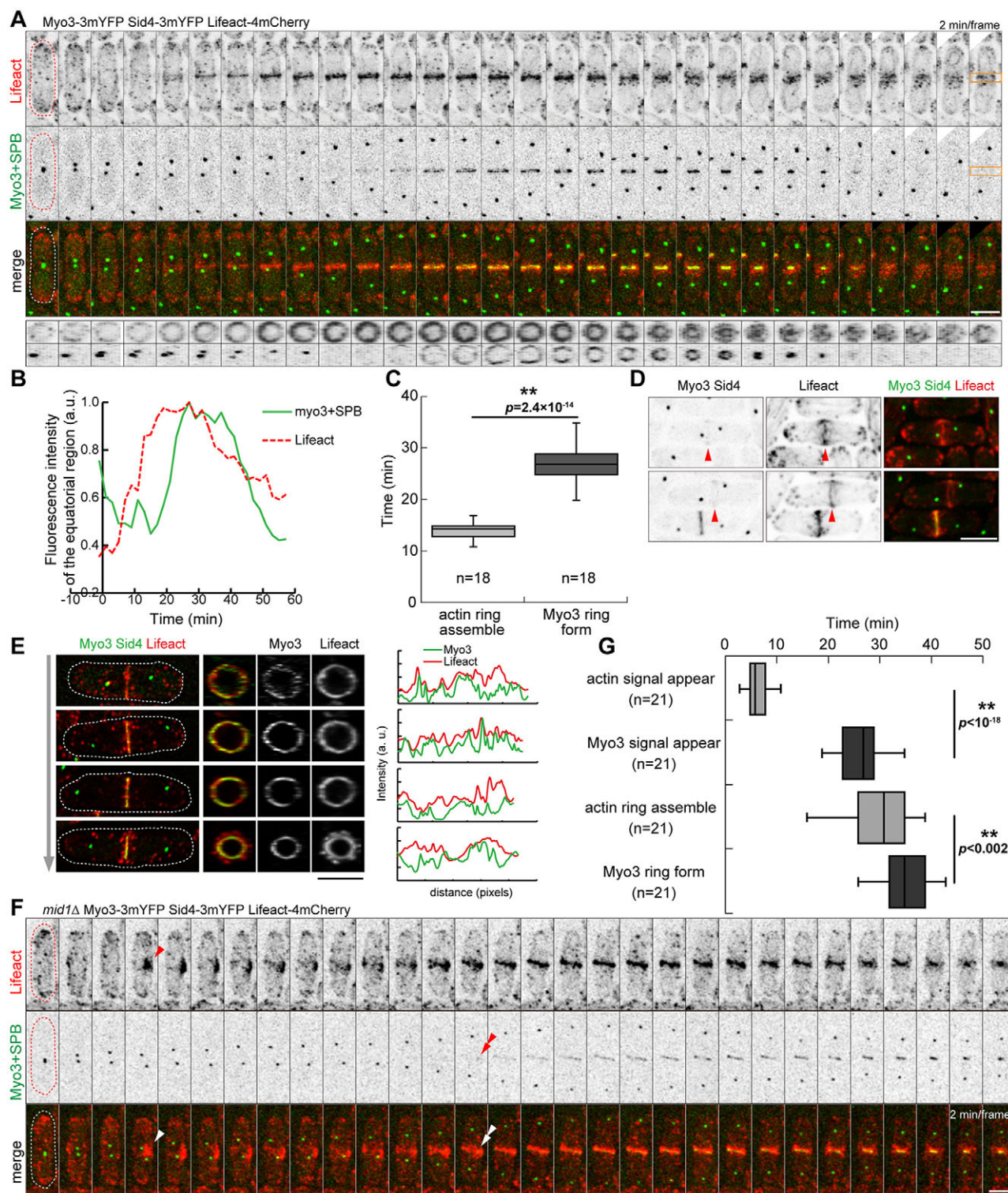
Fig. 2. Myo3 gradually localizes to the contractile ring during actin ring assembly. (A) Simultaneous observation of Myo3 and actin during assembly and constriction of the contractile ring. Bottom, images obtained from 90° rotation of the medial region. (B) Mean fluorescence intensities of the boxed region in A were plotted over time. SPB separation was set as *t*=0. (C) Box plot of times required for the assembly of actin and Myo3 rings from SPB separation. Data were pooled from two independent preparations. (D) Myo3 hardly localizes to the actin ring under construction. The precursor fine F-actin was visualized by higher speed image acquisition. Arrowheads indicate unassembled actin rings. Note that a very weak signal of Myo3–3mYFP in unassembled actin rings may not have been detected in A due to the lower detection limit of the system used in that experiment. (E) An orthogonal view of Myo3 and actin rings. Cells at progressive stages of Myo3 accumulation were imaged with higher spatial resolution. Right, line profiles of actin and Myo3 fluorescence intensities along the circumference. (F) Simultaneous observation of Myo3 and actin during cytokinesis in *mid1Δ* cells. The arrowhead indicates the appearance of a clump of actin strands. The double arrowhead indicates appearance of the Myo3 signal. (G) Box plot of times required for the assembly of actin and Myo3 rings in *mid1Δ* cells. Data were pooled from three independent preparations. **P<0.01. Scale bars: 5 μm.
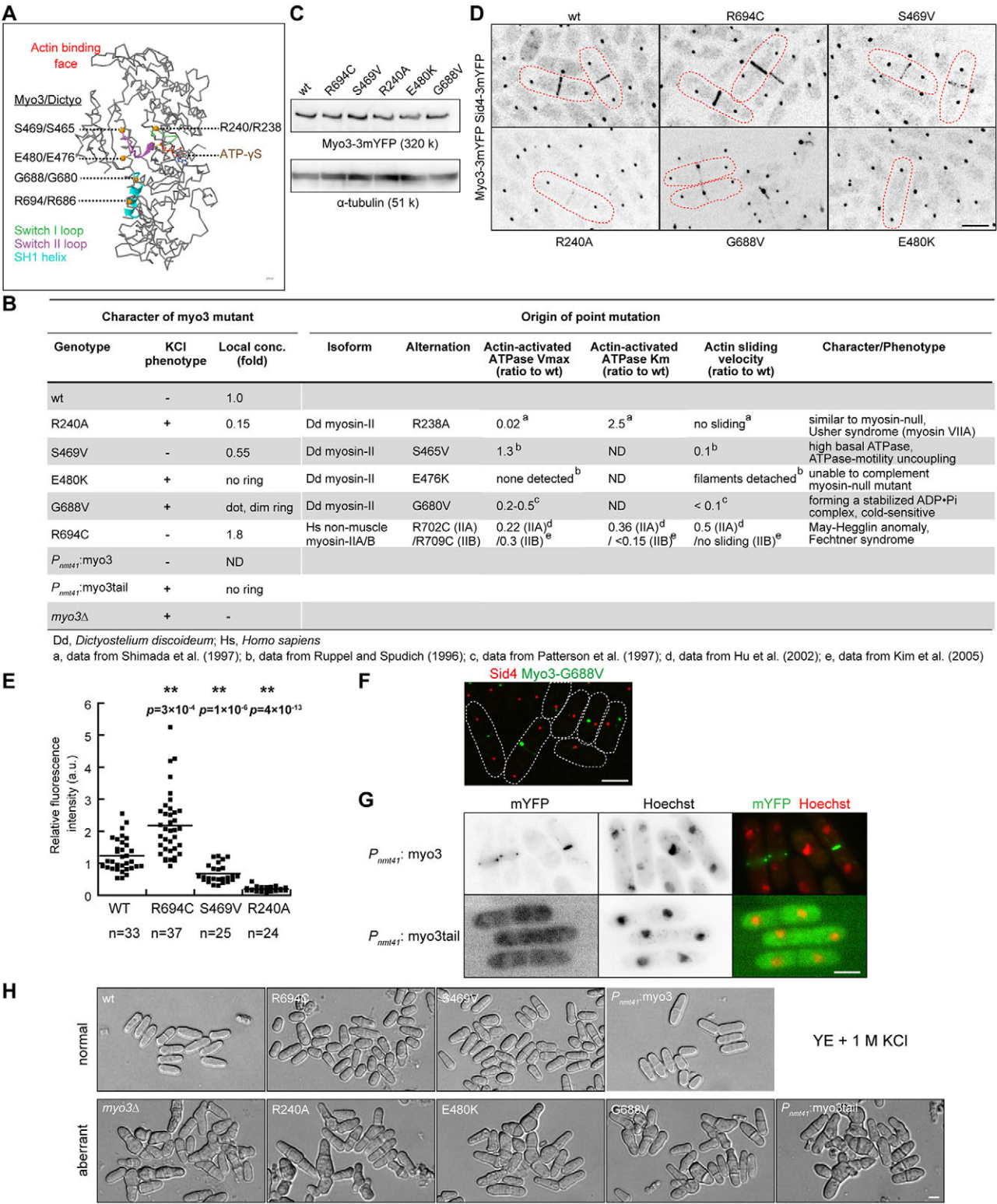
Fig. 3. Localization and functions of mutant Myo3 proteins. (A) Positions of the point mutations introduced into Myo3 are indicated on the structure of *Dictyostelium* myosin-II head (PDB code: 1MMG) drawn by Jmol. (B) Summary of the functions and local concentrations of the mutant Myo3 proteins, and characteristics of the original point mutations (see also supplementary material Fig. S1). (C) A western blot analysis of the protein levels of wt and mutant Myo3 proteins. Myo3–3mYFP was detected as a 320-kDa band by an anti-GFP antibody. The levels of α-tubulin are shown as a loading control. (D) Localization of wt and mutant Myo3 proteins in late anaphase cells. (E) Dot plot of fluorescence intensities of the mutant Myo3–3mYFP rings (see Materials and Methods). Data were pooled from three independent experiments. Horizontal lines indicate the means. **$P < 0.01$ compared with wt. (F) Cells expressing Myo3-G688V–3mYFP and Sid4–3mCherry were imaged. (G) The localization of Myo3 and the Myo3 tail expressed under the control of the *nmt41* promotor. Cells were grown in the presence of 5 μM thiamine and then imaged in a single focal plane. (H) Cells expressing wt and mutant Myo3 proteins were grown in the presence of 1 M KCl. Scale bars: 5 μm.
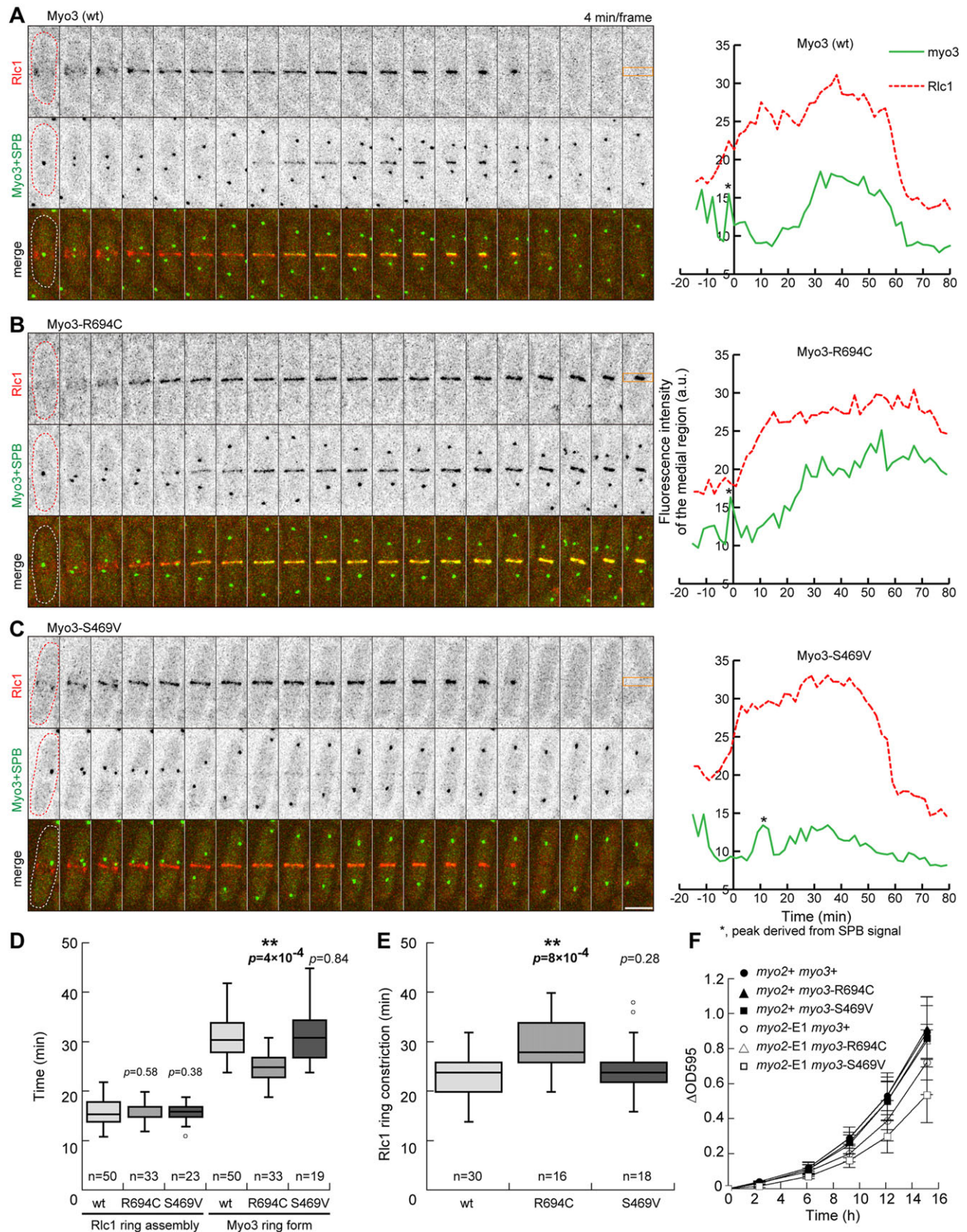
Fig. 4. Accumulation kinetics of mutant Myo3 proteins during cytokinesis. (A–C) Simultaneous observation of Rlc1 and Myo3 (A), Myo3-R694C (B) or Myo3-S469V (C) during assembly and constriction of the contractile ring. Right, mean fluorescence intensities of the medial region (boxed) were plotted over time. (D,E) Box plots of times required for the assembly of Rlc1 and mutant Myo3 rings from the SPB separation. (E) Box plot of the time required for constriction of the Rlc1 ring. Data in D and E were pooled from two independent preparations. **P<0.01 compared with wt. (F) Growth curves of wt and mutant *myo3-3mYFP* cells cultivated at 25°C. Data are the mean±s.d. from three independent measurements. Scale bars: 5 μm.

We also examined the localization of the C-terminal tail (amino acids 827–2104) of Myo3. An mYFP-tagged Myo3tail (Myo3tail–3mYFP) expressed under the control of the *nmt41* promoter diffused throughout the cytoplasm, whereas full-length Myo3 expressed under the same promoter localized to the contractile ring (Fig. 3G). This result again suggests that Myo3 localizes to the cytokinetic actin ring in a manner that depends on its head moiety.

Myo3-null cells show a morphological phenotype in the presence of high concentrations of the Cl⁻ ions, possibly because of the failure of cytokinesis (Bezanilla et al., 1997; Motegi et al., 1997). Therefore, we investigated the Cl⁻ ion sensitivity of mutant *myo3* strains. Cells from E480K, R240A, G688V and myo3tail mutants were often multi-septated and swollen in 1 M KCl, similar to *myo3Δ* cells, whereas cells from *myo3⁺*, S469V and R694C strains showed no morphological defects (Fig. 3H). Therefore, the function of *myo3⁺* to maintain cell morphology under high Cl⁻ ion conditions might require its local concentration to the contractile ring to be higher than a minimum level, but does not appear to correlate with its motor activity.

Accumulation kinetics of mutant Myo3 proteins during cytokinesis

We next examined the S469V and R694C mutants because they did not exhibit the KCl phenotype, but had a lower or higher local concentration to the contractile ring, respectively, than wt. We observed the accumulation of wt or mutant Myo3 together with Rlc1, a light chain of myosin-II, during cytokinesis. Rlc1 colocalized with Myo2 and Myo3, and could be used to visualize the course of contractile ring assembly from a band of cortical nodes in the medial region. The wt Myo3 formed a medial ring ∼15 min after the Rlc1 ring had assembled (Fig. 4A,D; supplementary material Movie 4). Myo3-R694C accumulated on the contractile ring earlier than wt and decelerated constriction of the ring (Fig. 4B,D,E; supplementary material Movie 4). Myo3-S469V accumulated on the ring with kinetics similar to those of wt; however, its local amount was markedly lower, and did not interfere with ring constriction (Fig. 4C–E). Neither of the mutant Myo3 proteins retarded the cell growth (Fig. 4F) or assembly of the contractile ring, as monitored by Rlc1 localization (Fig. 4D) in *myo2⁺* strains. These results suggest that binding sites for Myo3 on the ring are available after the completed assembly of the ring, and diffused Myo3 molecules directly bind to the sites rather than migrating towards the ring through ring-associated actin tracks (Arai and Mabuchi, 2002; Huang et al., 2012).

Myo3 is involved in the constriction rate of the contractile ring and septation efficiency

The deceleration of ring constriction by the Myo3-R694C mutant implied the involvement of Myo3 in ring constriction during cytokinesis under normal conditions, as reported recently (Arasada and Pollard, 2014), and not only under severe conditions (Bezanilla et al., 1997; Motegi et al., 1997). Therefore, we re-examined the phenotypes of *myo3Δ* under normal growth conditions. The percentage of singly septated cells was significantly higher in an asynchronous culture of *myo3Δ* than in wt, suggesting prolonged cell division (supplementary material Fig. S2A,B). We also observed that the rate of constriction of the contractile ring in *myo3Δ* cells was significantly lower (80%) than that in wt cells, whereas the time required for ring assembly and the dwell time of the contractile ring were similar in both strains (supplementary material Fig. S2C–E). These results imply that Myo3 is involved in the constriction of the contractile ring and,

hence, show that it is required for efficient septation under normal conditions.

Stable localization of Myo3 to the contractile ring is required for its maintenance in the *myo2-E1* background

In order to understand the function of Myo3 in cytokinesis in more detail, we examined motor-impaired *myo3* mutants in the *myo2-E1* background, a temperature-sensitive mutant strain of *myo2* that shows severe defects in contractile ring assembly at a restrictive temperature (Balasubramanian et al., 1998) and slower assembly and constriction of the ring at a permissive temperature (Stark et al., 2010). Biochemically, the mutant Myo2 has significantly diminished ATPase activities and is unable to drive the gliding of F-actin, but binds to filaments under restricted diffusion conditions (Stark et al., 2013). We generated *myo2/myo3* double mutants and observed contractile ring assembly at 25°C. In *myo2-E1 myo3⁺* cells, the assembly and constriction of the contractile ring were both slower than those in *myo2⁺* cells (compare Fig. 4A,D,E and Fig. 5A,E,F). Prolonged ring assembly also delayed the localization of Myo3 to the contractile ring. In *myo2-E1 myo3-R694C* cells, constriction of the contractile ring was retarded more than that in *myo2-E1* cells, indicating that Myo2-E1 and Myo3-R694C additively affect ring constriction (Fig. 5B,E,F). Myo3-R694C localized to the contractile ring earlier than Myo3, as observed in *myo2⁺* cells. Although Myo3-S469V–3mYFP localized to the contractile ring in the *myo2-E1* background, its signal was very susceptible to photobleaching (supplementary material Fig. S3A), and, thus, we were unable to precisely determine when the Myo3-S469V ring was formed. The contractile ring constricted slower in 44% of *myo2-E1 myo3-S469V* cells than in *myo2-E1* cells (Fig. 5C–F; supplementary material Movie 5). In half of the cells, the ring signal of the Rlc1 gradually degraded after late anaphase, and septation was retarded (Fig. 5C,D,G; supplementary material Movie 6). This was unexpected because more than 95% of cells in the *myo2-E1* and *myo2-E1 myo3-R694C* strains showed constriction of the ring, and no ring degradation was observed. Furthermore, the rings that assembled were deformed in 45% of *myo3-S469V* cells (arrowheads in Fig. 5C,H,I). Correspondingly, the growth of *myo2-E1 myo3-S469V* cells was slightly slower (Fig. 4F). The contractile ring assembled with similar kinetics in these three strains. These results suggest that the motor activities of Myo2 and Myo3 are jointly involved in maintaining the contractile ring after anaphase.

We also examined the behavior of the actin ring in *myo2-E1 myo3-S469V* cells (supplementary material Fig. S3). Most *myo2-E1* cells septated after the medial actin ring constricted. The actin ring constricted more slowly in 50% of *myo2-E1 myo3-S469V* cells than in *myo2-E1* cells, and delayed septation occurred. In the remaining cells, the actin ring assembled, but then decondensed into fragments, and septation was also retarded. Collectively, we conclude that actin and myosin-II structures in the contractile ring might both be decomposed in half of the *myo2-E1 myo3-S469V* cells. Taken together, these results suggest that catalytically active myosin-II motors contribute to the maintenance of actin and myosin structures in the contractile ring.

cdc8 genetically interacts with *myo3*

Cdc8 is the single tropomyosin of fission yeast and is essential for the cytokinesis and organization of the actin cytoskeleton (Balasubramanian et al., 1992; Chang et al., 1996), and has been shown to localize to F-actin cables and the contractile ring (Arai et al., 1998). Biochemically, Cdc8 stabilizes F-actin, enhances the association between Myo2 and F-actin, and promotes the actin-
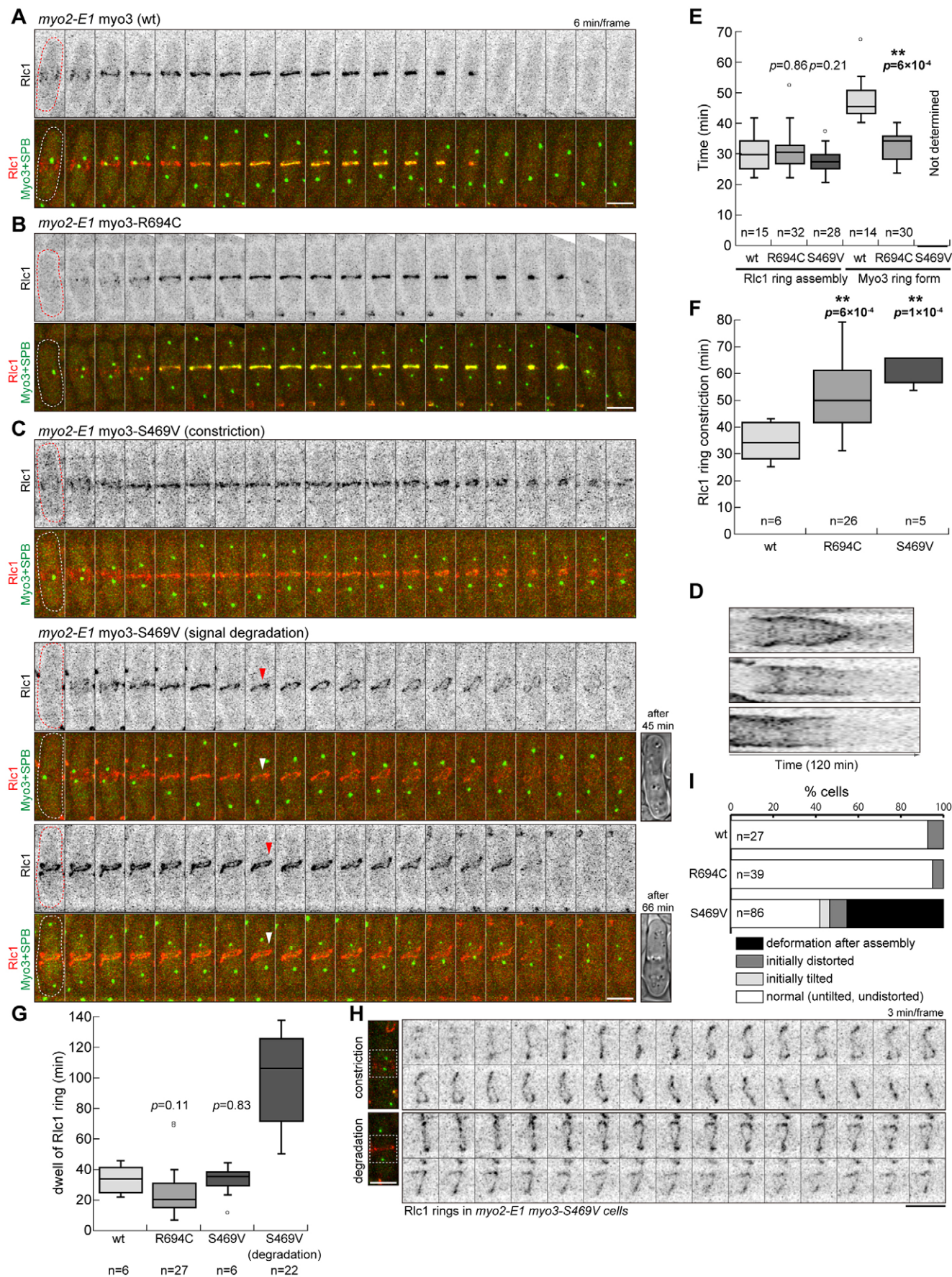
Fig. 5. See next page for legend.

Fig. 5. Sufficient accumulation of Myo3 to the contractile ring is required for its maintenance in the *myo2-E1* background. (A–C) Simultaneous observation of Rlc1 and Myo3 (A), Myo3-R694C (B) or Myo3-S469V (C) during assembly and constriction of the contractile ring in the *myo2-E1* background. Arrowheads indicate the onset of ring deformation. (D) Kymographs of the Rlc1 rings shown in C. (E) Box plots of times required for the assembly of Rlc1 and mutant Myo3 rings from the SPB separation. (F) Box plot of the time required for constriction of the Rlc1 ring. (G) Box plot of the duration of unconstricted rings. (H) Deformation of Rlc1 rings in *myo2-E1 myo3-S469V* cells. Boxed regions of the cells are magnified 1.5 times. (I) The rings in the cells of indicated genotypes were scored according to their deformation. Data in E–G and I were pooled from two to four independent experiments. **$P<0.01$ compared with wt. Scale bars: 5 μm.

activated ATPase activities of Myo2 (Stark et al., 2010). Therefore, we generated and examined a double mutant bearing both *myo3Δ* and *cdc8-110*, a temperature-sensitive mutant of *cdc8* (Nurse et al., 1976). Under all permissive temperatures tested, *myo3Δ cdc8-110* cells grew more slowly than wt and single mutants (supplementary material Fig. S4A). Moreover, the number of multinucleated cells was significantly higher in the double mutant than in the single mutants (supplementary material Fig. S4B). These results indicate that *myo3* and *cdc8* are synergistically involved in cytokinesis and cell growth and are consistent with previous findings (Motegi et al., 1997). We also examined the assembly and constriction of the contractile ring in the double mutant under permissive conditions. The time required for assembly of the contractile ring was longer in *cdc8-110* and *myo3Δ cdc8-110* cells, by ~7 min, than in wt or *myo3Δ* cells (Fig. 6A,B,D), suggesting that there is no cooperativity between *myo3* and *cdc8* for ring assembly. However, there appeared to be significant cooperativity for ring constriction and ring maintenance. The ring constricted very slowly in 32% of the double mutant cells, whereas in most of the wt, *myo3Δ* and *cdc8-110* cells the ring constricted much faster (Fig. 6C,E,F). In 44% of *myo3Δ cdc8-110* cells, the ring persisted for an abnormally long time (at least 70 min, the maximum lifetime of the contractile ring in wt) without constriction (Fig. 6C,E,F). This long-lasting ring was also observed in 4% of *cdc8-110* cells. The ring disappeared after an unusually prolonged duration without constriction in 20% of the double mutant cells (Fig. 6E,F; supplementary material Movie 7). In addition, 35% of *myo3Δ cdc8-110* cells displayed a deformed contractile ring after its assembly (Fig. 6G,H), which was not observed in other strains or resembled *myo2-E1 myo3-S469V* cells. These results suggest that *myo3* cooperates with *cdc8* to properly maintain the contractile ring after late anaphase, and are partially supportive of the aforementioned hypothesis that myosin motors contribute to maintaining the contractile ring.

Myo3 formed motile clusters on the ring

We attempted to elucidate the mechanism responsible for the Myo3-mediated maintenance of the contractile ring. Fluorescence recovery after the photobleaching (FRAP) analysis revealed that Myo3 at the contractile ring was largely immobile and turned over relatively slowly (Fig. 7A,B), which indicates the stable localization of Myo3 and is consistent with its function as a ring stabilizer. Myo3-R694C had a smaller mobile fraction and turned over more slowly than wt, again suggesting that ATP hydrolysis correlated with the dissociation of Myo3 from the ring.

In order to gain further insights into the behavior of Myo3, we investigated the discontinuous signals of Myo3–3mYFP at the contractile ring (as described in Fig. 2) using time-lapse imaging. The signals of Myo3–3mYFP gradually accumulated as dozens of fine dots along the actin ring and formed a discontinuous ring

(Fig. 7C). Hereafter, we refer to these dots as Myo3 clusters. These clusters were constantly motile and their fluorescence intensities varied (Fig. 7D; supplementary material Movie 8). A kymographic analysis revealed that the Myo3 clusters continually emerged and disappeared, with an average lifetime of 29 s, and were capable of moving in both directions (Fig. 7F). Myo3-R694C–3mYFP formed slightly more clusters than wt, and they had significantly longer lifetimes (Fig. 7E,F; supplementary material Movie 8), which is consistent with the higher local concentrations and low mobility.

We constructed several deletion forms of Myo3–3mYFP (Fig. 7G) in order to identify the regions involved in the clustering or localization of Myo3. The C-terminal coiled-coil region spanning 500 amino acids was dispensable for localization to the contractile ring and cluster formation (Fig. 7H). Deletions including the central region of the tail moiety (corresponding to amino acids 1248–1615) significantly decreased the medial accumulation of Myo3: Myo3-1048 localized as dim puncta along the equator, and Myo3-1247 and Myo3-827 sometimes accumulated as several dots in the medial region. We also found that the moderate expression of Myo3-1248-1615–3mYFP did not localize to the contractile ring (Fig. 7I). When overexpressed, Myo3-1248-1615 localized weakly to the equator in late anaphase cells. Most of the deletion forms of Myo3–3mYFP localized similarly in *myo2-E1* strains (supplementary material Fig. S4D), which means it is unlikely that they are recruited through interactions with Myo2. Taken together, these results suggest that Myo3 molecules form multimeric complexes on the contractile ring and that the medial localization of Myo3 depends on the motor domain and central region of the tail.

We then investigated the biochemical properties of Myo3-1248-1615 using a sedimentation assay. GST–Myo3-1248-1615 alone partially sedimented, whereas GST did not (Fig. 8A). F-actin significantly increased the amount of sedimentable GST–Myo3-1248-1615 (Fig. 8B). These results indicate that Myo3-1248-1615 is more likely to form large aggregates or interacts with F-actin weakly with an apparent K_d of 7±2 μM.

DISCUSSION
The motor properties of Myo3 are relevant to its distribution over the ring and its local concentration
The contribution of the motor domain of myosin-II proteins to their localization to the cleavage furrow or the contractile ring had previously been unclear because the accumulation of myosin-II to the cleavage furrow or contractile ring was typically concurrent with its filamentogenesis and depended heavily on the tail moiety, but not on the motor domain (Dean et al., 2005). Some scaffold proteins might tether the rod of myosin-II filaments to the equatorial cortex in these cells. In the present study, we showed that Myo3 localized to the contractile ring by solely depending on F-actin throughout cytokinesis and that its motor properties were relevant to its accumulation. The local concentrations of mutant Myo3 proteins (R240A, E480K and R694C) correlated with the affinity of the head for F-actin in the presence of ATP, as represented by the K_m value. The reduced local concentration of Myo3-S469V to the contractile ring might also have been due to its lower affinity for F-actin because a similar uncoupling mutant S456L appears to have a higher K_m value for actin than that of wt (Murphy et al., 2001). In addition, the clumping of Myo3-G688V suggests that an uninterrupted ATP hydrolysis cycle is required for uniform distribution along the ring. In contrast, the motility of the mutant Myo3 did not appear to directly correlate with its localization. A cycle of ATP hydrolysis by myosin-II is coupled to a cycle of
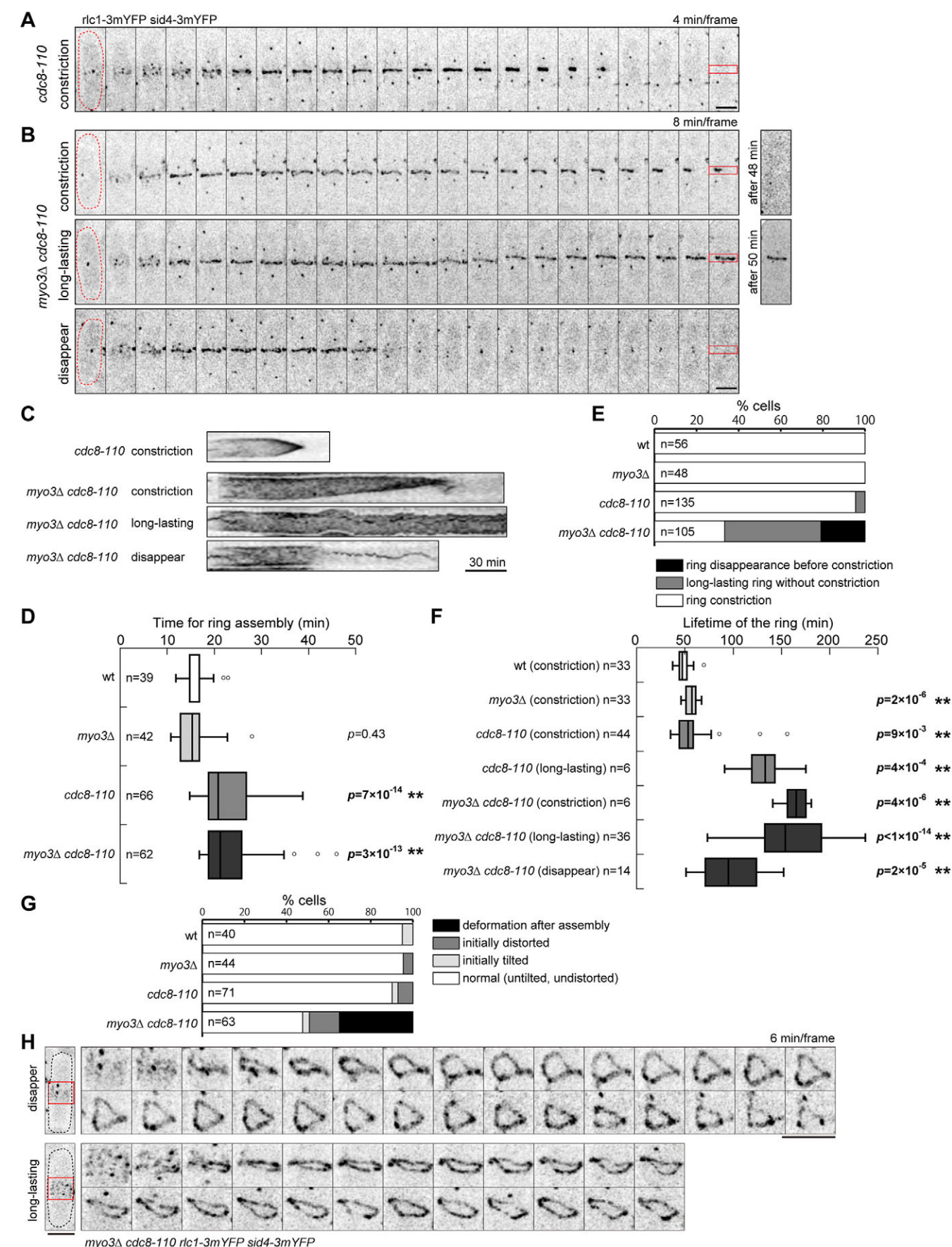
Fig. 6. See next page for legend.

Fig. 6. Synthetic genetic interaction between *myo3* and *cdc8*. (A,B) Time-lapse imaging of the assembly and constriction of Rlc1 rings in *cdc8-110* (A) and *myo3Δ cdc8-110* (B) cells. (C) Kymographs of the boxed regions shown in A and B. (D) Box plot of the times required for the assembly of Rlc1 from the SPB separation. (E) The Rlc1 rings in the cells of the indicated genotypes were scored according to their behaviors. (F) Box plot of the lifetime of the Rlc1 ring from its assembly to the disappearance of its signal. (G) Rlc1 rings were scored according to their deformation. Data in D–G were pooled from two to five independent experiments. (H) Deformation of the rings in *myo3Δ cdc8-110* cells. Boxed regions of the cells are magnified two times. **$P<0.01$ compared with wt. Scale bars: 5 μm.

attachment to and detachment from F-actin. Thus, disassociation by ATP hydrolysis from F-actin rather than motility might be essential for spreading Myo3 over the contractile ring. All of the point mutations introduced into Myo3 were located outside the actin-binding face of the motor domain and, hence, were less likely to directly alter its affinity for F-actin.

The motor domain of Myo2 localizes solely to the contractile ring (Lord et al., 2005), and Myo3-1048 also accumulated along the ring, suggesting the specific association of myosin-II motor domains with contractile ring F-actin. One possible mechanism for this is the preferential binding of myosin-II motor domains to mechanically stretched F-actin (Uyeda et al., 2011). Myo3 was hardly detectable on precursor medial reticular F-actin, whereas it accumulated along the sharp actin ring, which implies that the configuration or tension of the equatorial F-actin affects its affinity for Myo3. The fact there is an inefficient equatorial accumulation of Myo3-827 in the *myo2-E1* strain (in which tension could be weakened) might also support this idea. Alternatively, actin-binding proteins associating with contractile ring F-actin might increase the affinity of myosin-II for actin, as previously reported for Cdc8 (Stark et al., 2010).

Myo3 cooperated with Myo2 and Cdc8 to maintain the actin ring after late anaphase

The motor activity of myosin-II might drive the shrinkage of interdigitated F-actin in the contractile ring (the purse-string model). Our results suggest that myosin-II motor activity was also vital for maintaining the contractile ring, providing a new perspective regarding the functions of myosin-II in cytokinesis (Fig. 8C). Maintenance of the contractile ring evidently underpins its constriction because destabilization, or even disassembly, of the ring either before or during constriction is unfavorable. After being joined to the ring at late anaphase, Myo3 might collaborate with Myo2 in its maintenance and constriction. Based on the functional equivalency of the motor heads between Myo3 and Myo2 (Bezanilla and Pollard, 2000), the two myosin-II proteins might work in parallel using a similar mechanism. Given that half of the *myo2-E1 myo3-S469V* cells displayed constriction of the contractile ring, whereas the other half did not, a minimum requirement (i.e. a watershed, proportional to their local concentrations and specific ATPase activities) appears to exist for ring-localized myosin-II motor activity that is necessary in order to maintain the ring. The amount of myosin-II activity might be very close to the minimum in these cells. Given that *myo3-S469V* cells did not exhibit a morphological phenotype in 1 M KCl, maintenance of the contractile ring might be the primary role of Myo3, which could be separate from its role in tolerance of high concentrations of the Cl⁻ ion. Assuming that a signaling cascade is activated under high-Cl⁻ ion conditions, it is possible that Myo3 provides a scaffold for signal transduction in which signaling molecules interact, as has already been speculated (Bezanilla and Pollard, 2000).

We also found that maintenance of the contractile ring was compromised in *cdc8-110 myo3Δ* cells, in which the activity of myosin-II proteins was presumably reduced. Cdc8 might indirectly enhance the actin–myosin interaction and ATPase activity of Myo2 (and possibly Myo3) in order to properly maintain the contractile ring after late anaphase. Double mutant cells also displayed unusual persistence of the contractile ring. The small fraction of *cdc8-110* cells with a long-lasting ring indicates that the initiation of ring constriction is mechanically unfavorable, which might be exaggerated in combination with *myo3Δ*. We speculate that Cdc8 also stabilizes the actin ring through direct binding in order to maintain the ring to some extent and promote transition from the dwell phase to constriction.

Possible mechanisms responsible for Myo3-mediated maintenance of the actin ring

A previous study has demonstrated that the recombinant Myo3 tail is monomeric because it formed an intramolecular coiled-coil and, hence, Myo3 is a single-headed myosin-II (Bezanilla and Pollard, 2000). However, contractile-ring-localized Myo3 might be in large assemblies because most of the Myo3 signal appeared as dozens of motile puncta. We also found that the motor domain of Myo3 and central region of its tail were both weakly localized to the medial cortex at late anaphase, and both were required for sufficient accumulation. Myo3 appeared to interact superficially with the actin ring rather than being integrated into the ring considering it is concentrated at the ring after F-actin. These results prompted us to speculate that Myo3 molecules on the actin ring formed clusters with their tails, which associate with a kernel (Fig. 8D). As the local amount of Myo3 has been estimated to be ∼2000 molecules (Wu and Pollard, 2005), each cluster might comprise several tens of Myo3 molecules. The Myo3 cluster might be able to sustain continuous attachment to the contractile ring F-actin and crosslink the filaments, either circumferentially or transversely, as it has multiple motor domains. The multivalent attachment of Myo3 clusters might contribute to consolidation of the actin ring. A FRAP analysis revealed the slow turnover rate and low mobility of ring-localized Myo3, which might be explained by its preferential incorporation into the clusters. Meanwhile, single-headed Myo3 would not be expected to interact with F-actin as persistently because it is presumed to have a very low duty ratio. Thus, clustering of Myo3 might be a suitable machinery to permit a single-headed myosin-II to maintain the contractile ring by associating stably with the actin ring.

The molecular entity of cluster kernels remains unknown. The transmembrane protein Chs2 localizes to the medial region during septation and co-immunoprecipitates with Myo3 (Martín-García and Valdivieso, 2006). However, given that Myo3 localizes to the contractile ring in *chs2Δ* cells, Chs2 might not provide a strong anchor for Myo3. Amino acids 1248–1615 of Myo3 might be directly involved in clustering on the actin ring because this moiety is liable to form aggregates, and F-actin might facilitate aggregation. Given that these properties and cellular localization appear to differ from those of the entire tail (Bezanilla and Pollard, 2000; Fig. 3G), this region might be structurally masked by other regions. Posttranslational modifications (e.g. phosphorylation) could relieve this masking.

Myo3-R694C maintained the contractile ring as effectively as Myo3 in the *myo2-E1* background, suggesting that the association between myosin-II proteins and F-actin might be more important for maintenance of the ring than their ATPase activity or motility. This is reminiscent of the situation in COS-7 cells (Ma et al., 2012) in which the mutant non-muscle myosin-II, human non-
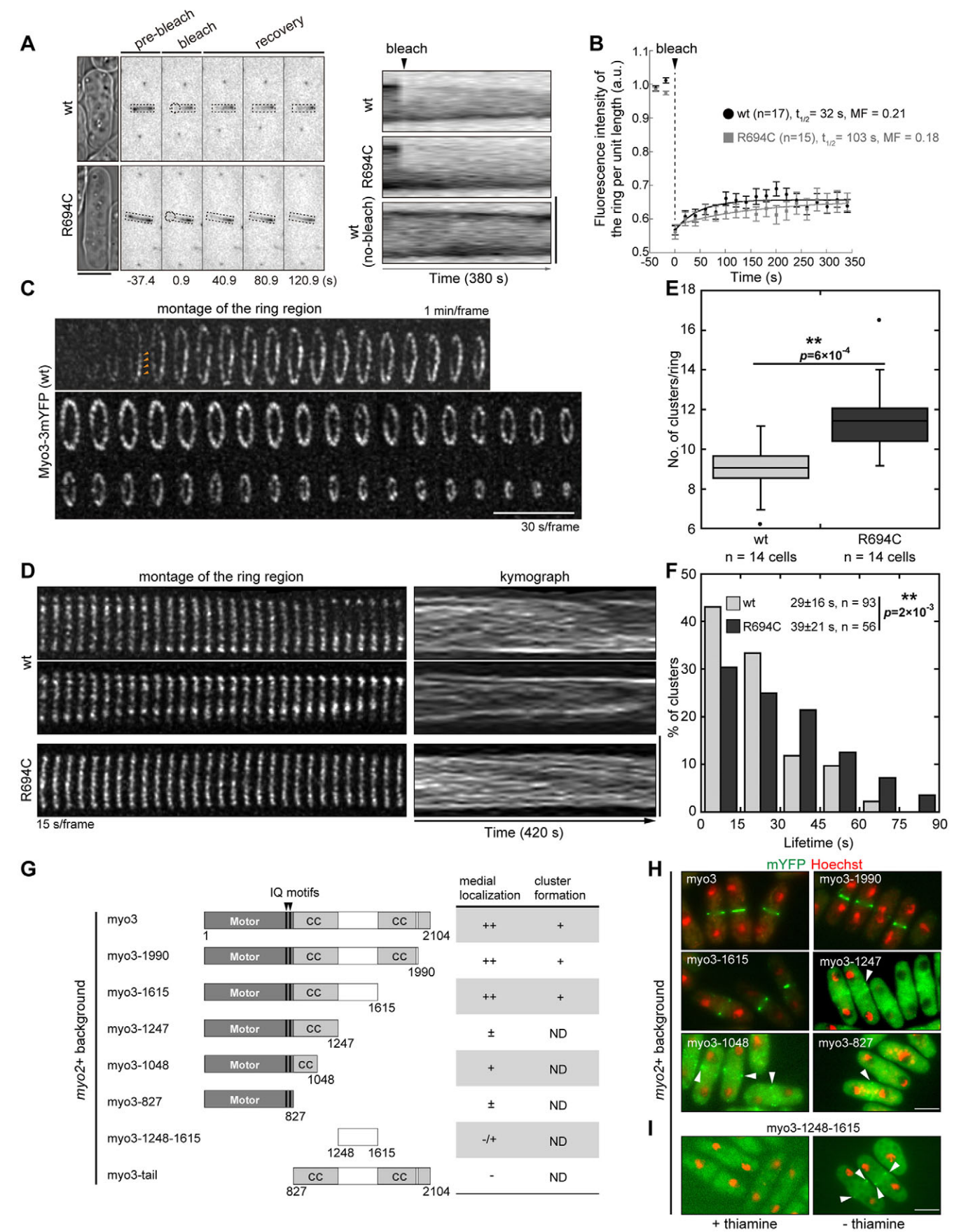
Fig. 7. See next page for legend.

Fig. 7. Myo3 formed motile clusters on the ring. (A) The ring of Myo3–3mYFP or Myo3-R694C–3mYFP (boxed regions) was photobleached at $t=0$ s on one side (in a circle) and imaged. Right, kymographs of the boxed region. (B) The fluorescence intensities of bleached regions were plotted over time. Data are the mean±s.e.m. plotted over time with best fit curves. (C) Slightly tilted *myo3-3mYFP sid4-3mYFP* cells were imaged. Maximum projections of *z*-stacked deconvolved images. Arrowheads indicate the emergence of Myo3 clusters. (D) Clusters of Myo3 and Myo3-R694C were examined by time-lapse imaging (see Materials and Methods). Right, kymographs of the ring region. (E) Box plot of the time-averaged number of Myo3 clusters detected per ring (see Materials and Methods). Data were pooled from four independent experiments. (F) The lifetime distribution of individual clusters. Data were pooled from three to four independent experiments. The mean±s.d. is shown. (G) Diagram of the *myo3* deletion forms. The localization of the mutant proteins in *myo2+* strains is summarized. Note that all these mutant forms were expressed from the original locus in place of the endogenous Myo3. ++, strong; +, some; ±, weak; -/+, localization depends on conditions; ND, not determined. (H) Cells expressing the indicated forms of Myo3–3mYFP were imaged in a single focal plane. (I) Myo3-1245-1615–3mYFP was expressed under the control of the *nmt41* promoter in the presence or absence of thiamine for 19–25 h. Arrowheads in H and I indicate the medial localization of mutant Myo3 proteins. Double asterisks indicate a significant difference. **$P<0.01$ compared with wt. Scale bars: 5 µm.

muscle myosin IIB R709C (equivalent to the R694C alternation), was able to support cytokinesis; however, it had significantly reduced ATPase activity and was unable to translocate F-actin. The proposal that bipolar myosin-II filaments are not required for their motor activity, to glide F-actin, but as an active actin crosslinker to generate cortical tension, which drives cytokinesis, appears to be consistent with our results. Moreover, our results are compatible with studies using *Dictyostelium* and protoplasts of fission yeast showing that the contractile ring maintains local cortical tension, but does not limit the speed of constriction (Reichl et al., 2008; Stachowiak et al., 2014). The greater importance of the local concentration of Myo3 over its motor activity for ring maintenance also supports this idea. One of the common roles of myosin-II in eukaryotic cell cytokinesis might be the relocatable crosslinking of F-actin, which would enable tension to be exerted on cortical F-actin, including the contractile ring, to maintain the ring.

By contrast, Myo3-R694C dominantly reduced the rate of contractile ring constriction, suggesting that Myo3 itself is involved in ring constriction. Excessive consolidation of the ring through Myo3 clusters and Myo2 filaments might decelerate ring constriction. Conversely, the knockdown of α-actinin, a longer actin crosslinker that localizes to the cleavage furrow, accelerates cytokinesis in NRK cells (Mukhina et al., 2007). Therefore, local concentrations of different types of actin crosslinkers might coordinately determine the optimal constriction rate of the contractile ring.

MATERIALS AND METHODS
Yeast strains and genetic manipulations
The fission yeast strains used in this study are listed in supplementary material Table S1. These strains were constructed by a PCR-based-gene-targeting method, a PCR sewing technique (Bähler et al., 1998; Matsuyama et al., 2000) and genetic crosses. The plasmids used in this study are listed in supplementary material Table S2. Cells were grown in complete yeast extract medium YES or in minimal medium EMM with auxotrophic supplements. Cells were grown to mid-log phase at 25°C before imaging unless otherwise noted.

In order to precisely determine the localization of Myo3, we integrated three tandem copies of the monomeric yellow fluorescent protein (mYFP, a monomeric variant of YFP with an A206K mutation) at the C-terminus of the *myo3* chromosomal locus. A *3mYFP-hphMX6* module flanked by homologous sequences (400–500 bp) was amplified using MTP19 (Takaine et al., 2014a) as a template for this purpose. The DNA fragment was

transformed into the wt strain MTY10, and transformants were selected for hygromycin resistance. The Myo3–3mYFP fusion was fully functional. In order to generate tail-truncated mutant strains of *myo3*, MTY1001, MTY1002, MTY1003, MTY1008 and MTY1004, *3mYFP-hphMX6* modules were amplified using appropriate primers, as described above, and inserted after amino acids 1990, 1615, 1247, 1048 and 827 of endogenous *myo3*, respectively.

Point mutations were created by oligonucleotide-directed mutagenesis using a TAKARA mutagenesis kit (TaKaRa) and appropriate primers on the plasmid MTP467 carrying the *myo3+* gene (Motegi et al., 1997), to generate mutant *myo3-3mYFP* strains. All plasmids were sequenced to confirm PCR fidelity. In a *myo3-3mYFP* strain (MTY465), a region of the *myo3* gene (corresponding to 400–2400 bp) was replaced with a *ura4+* module, yielding strain MTY672. A *myo3* fragment, corresponding to 0–4000 bp, carrying a point mutation (MTP461, 465, 466, 486 or 487) was linearized by a *PstI/ScaI* cut of the mutagenized plasmid and subjected to the transformation of MTY672. Colonies were selected for uracil auxotrophy on a plate containing 5-fluoroorotic acid. Correct integrations were confirmed by diagnostic PCR and sequencing.

Microscopy
Single time-point and epifluorescence microscopy was performed using an inverted fluorescence microscope (BX51; Olympus) equipped with a Plan-Apo 100×1.40 NA objective lens (Olympus) using U-MNIBA3 and U-MWIG3 filters (Olympus) and a cooled charge-coupled device (CCD) camera (ORCAII-ER-1394; Hamamatsu Photonics) using SimplePCI software (Compix, Inc.) at room temperature. Time-lapse imaging was performed under a confocal microscope (LSM 700; Carl Zeiss, Inc.) equipped with an alpha Plan-Apochromat 100×1.46 NA objective lens (Carl Zeiss, Inc.) or using an inverted fluorescence microscope (BX71; Olympus) equipped with a UPlanSApo 100×1.40 NA objective lens (Olympus), spinning-disk confocal scanner (CSU22; Yokogawa), piezo objective positioner (E-665; Physik Instrumente) and electron multiplying CCD camera (iXon 3 885; Andor) with excitation by 488-nm and 568-nm lasers using GFP and mCherry filters and MetaMorph software (version 7.7.5.0; Molecular Devices) at 25°C. In the latter system, simultaneous two-color imaging was performed using an emission beam splitter (Dual View; Roper Scientific). Cells for time-lapse imaging were typically immobilized on pads made from 20% gelatin and 5% low-melting agarose in medium, or were directly mounted on a slide for single time-point observations. Stacks of 12–17 confocal *z*-sections spaced by 0.3–0.5 µm were typically collected. Confocal *z*-sections were sometimes deconvolved using Huygens Essential software (version 4.5; Scientific Volume Imaging) based on the classic maximum likelihood estimation method. In order to distinguish ring signal degradation in *myo2-E1 myo3-S469V* cells from global fluorescence decay due to photobleaching during imaging, we only scored the cells where the Rlc1–3mCherry ring signal disappeared before the mean fluorescence intensity at each frame of the time-lapse image was significantly decreased due to photobleaching. Throughout this study, mitotic progression was monitored by the separation of spindle pole bodies (SPBs) labeled by Sid4–3mYFP, indicating elongation of the spindle. The images shown are maximum projections of an *xy* image of *z*-stacks unless otherwise noted.

In time-lapse imaging of motile Myo3 clusters on the contractile ring, the signals of myo3–3mYFP were imaged by collecting nine confocal *z*-sections spaced by 0.31 µm through only the lower half of the cell with a 15-s interval using the inverted fluorescence microscope equipped with the CSU22 spinning-disk confocal scanner (see above). Each *z*-section was an average of two images. The images were deconvolved to explicitly visualize each cluster. In order to compare the mean number of clusters on the ring in *myo3-3mYFP* and *myo3-R694C-3mYFP* cells, we semi-automatically detected clusters using the find maxima function of ImageJ. The number of clusters detected in each frame was averaged across all (29–36) frames.

We manually selected tracks in kymographs to measure the lifetimes of clusters and only further analyzed clusters that met the following criteria: (1) they were brighter than the background signals, (2) were able to be discriminated from neighboring signals, (3) were almost spherical, and (4) had an almost constant signal intensity through its duration.
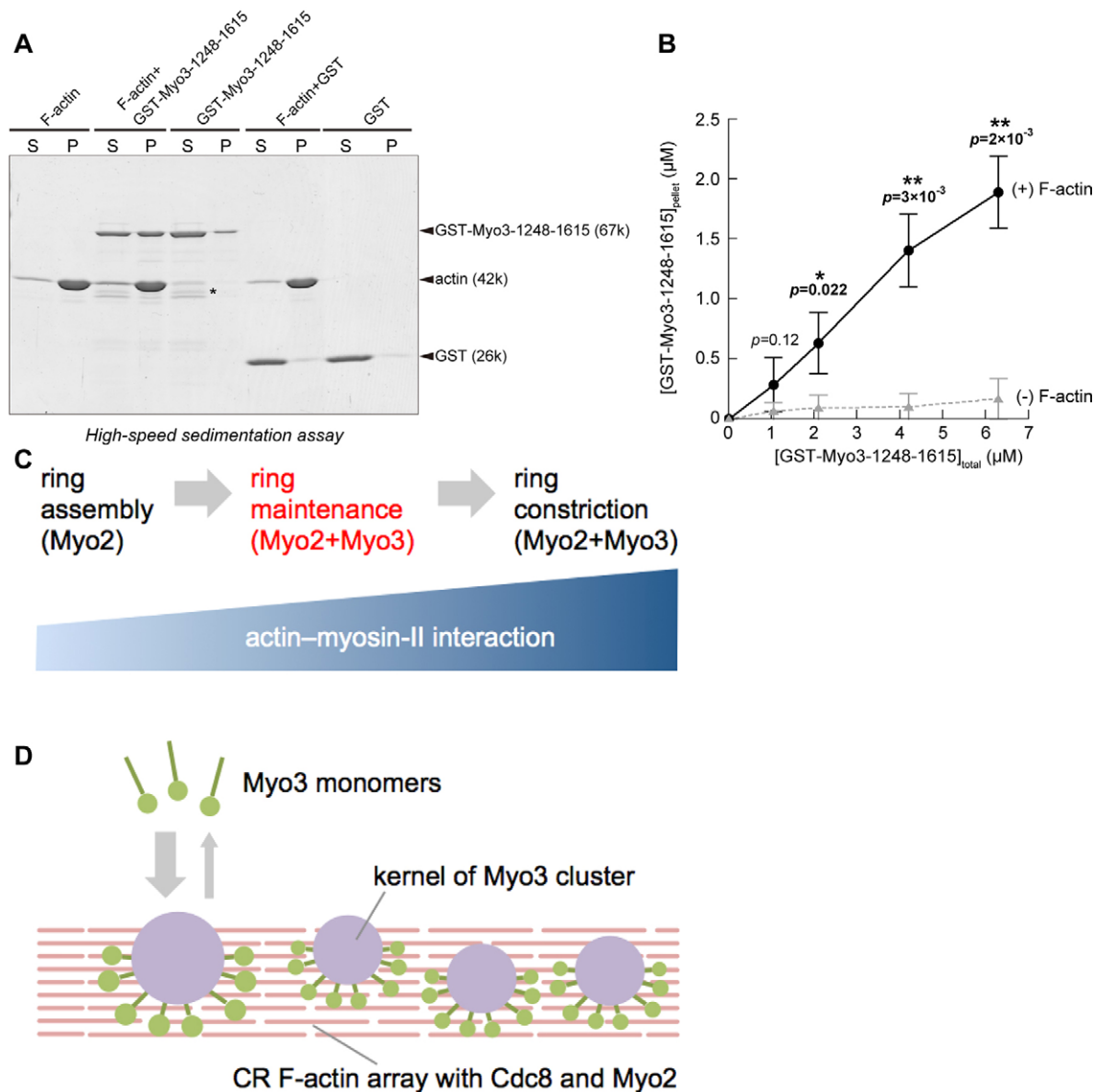
Fig. 8. Models for the function of the actin–myosin-II interaction and Myo3 during cytokinesis. (A) Sedimentation of GST, GST–Myo3-1248-1615 and F-actin. Samples were centrifuged, and the supernatant (S) and pellet (P) fractions were analyzed by SDS-PAGE. An asterisk indicates degradation products. (B) F-actin increased the amount of sedimentable Myo3-1248-1615. Several concentrations of GST–Myo3-1248-1615 were centrifuged in the absence and presence of F-actin, and the bands in the pellet fraction were quantified. Data are the mean±s.d. of three independent experiments. **$P<0.01$ compared with experiments without (−) F-actin. (C) Most Myo3 joins the contractile ring after its assembly, augmenting the net actin–myosin-II interaction in the ring. Myo3 and Myo2 maintain and then constrict the ring. Cdc8 enhances the actin–myosin-II interaction (not depicted). (D) A model for the localization and function of Myo3. CR, contractile ring.

FRAP measurements

Fluorescence recovery after the photobleaching (FRAP) analysis was performed using LSM 700 at 25°C. Stacks of 13 z-sections spaced by 0.5 µm were collected with a 20-s interval. Each z-section was an average of two images scanned using 0.5% laser power at 488 nm. Photobleaching was performed at 80% laser power by 20 iterative scanning in a circular region (20 pixels diameter) of the ring. Each z-stack was projected from an xy image using Image J and the sum intensity projection procedure. The mean fluorescence intensity of the ring region was measured, the background value was subtracted (an average of two cytoplasmic regions), and the result was normalized to the prebleach fluorescence intensity (an average of two time points before photobleaching). Data were further corrected for acquisition bleaching using the function, $I_t=I_\infty+(1-I_\infty)\times\exp(-k_{decay}\times t)$, where t is time, I_t is the normalized intensity at time point t, I_∞ is the normalized intensity at an infinite time point, and k_{decay} indicates a decay constant. The decay function was calculated by fitting the data from the unbleached ring regions using Kaleidagraph software (Synergy Software). The resultant recovery curve was fitted to a single exponential function, $I_t=I_\infty+(I_0-I_\infty)\times\exp(-k\times t)$, where I_0 is the normalized intensity just after bleaching, and k is the recovery rate constant closely related to the dissociation rate constant. The mobile fraction and half time ($\tau_{1/2}$) for recovery were calculated according to the equations mobile fraction=$(I_\infty-I_0)/(1-I_0)$ and $\tau_{1/2}=\ln 2/k$, respectively.

Quantitative fluorescence microscopy

Myo3–3mYFP ring intensities were quantified as previously described (Takaine et al., 2014a). In brief, we imaged *myo3-3mYFP sid4-3mYFP* cells in 13 z-sections at 0.38-µm intervals using the spinning disk confocal microscope averaging two images. The stack of z-sections was projected from an xy image using the sum intensity projection method of ImageJ. We then measured the mean fluorescence intensities of two SPBs and the medial rings in late anaphase cells. Regions of interests were a circle of 0.64 µm

(8 pixels) in diameter for one SPB and a rectangle of 0.5–1 µm (6–12 pixels)×2.4–4.0 µm (30–50 pixels) for the ring, respectively. After background subtraction, the total ring intensity was normalized to the average intensity of Sid4–3mYFP at SPBs in the cell.

Actin depolymerization assay using Lat-A

Cells for time lapse imaging were adsorbed onto the surface of a 35-mm glass-bottomed dish coated with lectin (L-2320, Sigma) for 10 min. The immobilized cells were imaged by collecting stacks of 12 z-sections spaced by 0.42 µm at 0.5- or 1-min intervals. During the interval after the second stack was acquired, the culture was supplemented with 0.36% DMSO alone or 0.36% DMSO and 5 µM Lat-A by the manual addition of an equal volume (approximately 50 µl) of the 2× concentrated solution. These cells were subsequently imaged until the F-actin signal disappeared. The mean fluorescence intensity of the medial region was measured, the background value subtracted, and the result was normalized to the pretreatment fluorescence intensity. Using Kaleidagraph software, the normalized decline curve was fitted to a single exponential function.

Immunoblotting

Total cell lysates were prepared from mid-log phase cells as described previously (Takaine et al., 2014b). Proteins were resolved by SDS-PAGE on 5–20% precast gels (C520L, ATTO) and transferred onto a polyvinylidene difluoride membrane (Immobilon-P; Millipore). YFP and α-tubulin were probed using an anti-GFP antibody (Roche) and the anti-tubulin antibody TAT-1 (Woods et al., 1989), respectively.

Actin sedimentation assay

Monomeric rabbit skeletal muscle actin, bacterially expressed recombinant GST, and GST–Myo3-1248-1615 were prepared as described previously (Takaine et al., 2009) and clarified by centrifugation at 200,000 g for 20 min. Samples containing 4 µM actin and 0–6.3 µM GST-Myo3-1248-1615 in KMEI (0.1 M KCl, 2 mM $MgCl_2$, 0.5 mM EGTA, 0.5 mM DTT, 0.2 mM ATP, and 10 mM imidazole-HCl, pH 7.5) were incubated for 30 min at 25°C, centrifuged at 200,000 g for 15 min, and the supernatants and pellets obtained were then subjected to SDS-PAGE. The gels were stained with Coomassie Blue, and bands were quantified by densitometry using Image J software.

Statistical analysis

Means, standard deviations and P-values were calculated using Excel software (Microsoft). Error bars denote s.d. unless otherwise noted. Significance between two sets of data was tested using an unpaired one-tailed Welch's t-test. These P-values are in bold type if the value was less than 0.05. Significance is also indicated by an asterisk. Box plots show the 75th and 25th percentiles of the data (interquartile range) as the upper and lower edges of the box, the median as the medial line in the box, the 1.5× interquartile range as whiskers, and outliers as circles.

References

Arai, R. and Mabuchi, I. (2002). F-actin ring formation and the role of F-actin cables in the fission yeast Schizosaccharomyces pombe. *J. Cell Sci.* **115**, 887-898.

Arai, R., Nakano, K. and Mabuchi, I. (1998). Subcellular localization and possible function of actin, tropomyosin and actin-related protein 3 (Arp3) in the fission yeast Schizosaccharomyces pombe. *Eur. J. Cell Biol.* **76**, 288-295.

Arasada, R. and Pollard, T. D. (2014). Contractile ring stability in S. pombe depends on F-BAR protein Cdc15p and Bgs1p transport from the Golgi complex. *Cell Rep.* **7**, 1533-1544.

Bähler, J., Wu, J.-Q., Longtine, M. S., Shah, N. G., McKenzie, A., III, Steever, A. B., Wach, A., Philippsen, P. and Pringle, J. R. (1998). Heterologous modules for efficient and versatile PCR-based gene targeting in Schizosaccharomyces pombe. *Yeast* **14**, 943-951.

Balasubramanian, M. K., Helfman, D. M. and Hemmingsen, S. M. (1992). A new tropomyosin essential for cytokinesis in the fission yeast S. pombe. *Nature* **360**, 84-87.

Balasubramanian, M. K., McCollum, D., Chang, L., Wong, K. C., Naqvi, N. I., He, X., Sazer, S. and Gould, K. L. (1998). Isolation and characterization of new fission yeast cytokinesis mutants. *Genetics* **149**, 1265-1275.

Bezanilla, M. and Pollard, T. D. (2000). Myosin-II tails confer unique functions in Schizosaccharomyces pombe: characterization of a novel myosin-II tail. *Mol. Biol. Cell* **11**, 79-91.

Bezanilla, M., Forsburg, S. L. and Pollard, T. D. (1997). Identification of a second myosin-II in Schizosaccharomyces pombe: Myp2p is conditionally required for cytokinesis. *Mol. Biol. Cell* **8**, 2693-2705.

Carvalho, A., Desai, A. and Oegema, K. (2009). Structural memory in the contractile ring makes the duration of cytokinesis independent of cell size. *Cell* **137**, 926-937.

Chang, F., Woollard, A. and Nurse, P. (1996). Isolation and characterization of fission yeast mutants defective in the assembly and placement of the contractile actin ring. *J. Cell Sci.* **109**, 131-142.

Dean, S. O., Rogers, S. L., Stuurman, N., Vale, R. D. and Spudich, J. A. (2005). Distinct pathways control recruitment and maintenance of myosin II at the cleavage furrow during cytokinesis. *Proc. Natl. Acad. Sci. USA* **102**, 13473-13478.

Eggert, U. S., Mitchison, T. J. and Field, C. M. (2006). Animal cytokinesis: from parts list to mechanisms. *Annu. Rev. Biochem.* **75**, 543-566.

Endow, S. A. (2000). Molecular motors–a paradigm for mutant analysis. *J. Cell Sci.* **113**, 1311-1318.

Ganem, N. J., Storchova, Z. and Pellman, D. (2007). Tetraploidy, aneuploidy and cancer. *Curr. Opin. Genet. Dev.* **17**, 157-162.

Goyal, A., Takaine, M., Simanis, V. and Nakano, K. (2011). Dividing the spoils of growth and the cell cycle: the fission yeast as a model for the study of cytokinesis. *Cytoskeleton* **68**, 69-88.

Guha, M., Zhou, M. and Wang, Y.-L. (2005). Cortical actin turnover during cytokinesis requires myosin II. *Curr. Biol.* **15**, 732-736.

Haviv, L., Gillo, D., Backouche, F. and Bernheim-Groswasser, A. (2008). A cytoskeletal demolition worker: myosin II acts as an actin depolymerization agent. *J. Mol. Biol.* **375**, 325-330.

Hu, A., Wang, F. and Sellers, J. R. (2002). Mutations in human nonmuscle myosin IIA found in patients with May-Hegglin anomaly and Fechtner syndrome result in impaired enzymatic function. *J. Biol. Chem.* **277**, 46512-46517.

Huang, J., Huang, Y., Yu, H., Subramanian, D., Padmanabhan, A., Thadani, R., Tao, Y., Tang, X., Wedlich-Soldner, R. and Balasubramanian, M. K. (2012). Nonmedially assembled F-actin cables incorporate into the actomyosin ring in fission yeast. *J. Cell Biol.* **199**, 831-847.

Kamasaki, T., Osumi, M. and Mabuchi, I. (2007). Three-dimensional arrangement of F-actin in the contractile ring of fission yeast. *J. Cell Biol.* **178**, 765-771.

Kim, K.-Y., Kovács, M., Kawamoto, S., Sellers, J. R. and Adelstein, R. S. (2005). Disease-associated mutations and alternative splicing alter the enzymatic and motile activity of nonmuscle myosins II-B and II-C. *J. Biol. Chem.* **280**, 22769-22775.

Lord, M., Laves, E. and Pollard, T. D. (2005). Cytokinesis depends on the motor domains of myosin-II in fission yeast but not in budding yeast. *Mol. Biol. Cell* **16**, 5346-5355.

Ma, X., Kovács, M., Conti, M. A., Wang, A., Zhang, Y., Sellers, J. R. and Adelstein, R. S. (2012). Nonmuscle myosin II exerts tension but does not translocate actin in vertebrate cytokinesis. *Proc. Natl. Acad. Sci. USA* **109**, 4509-4514.

Martín-García, R. and Valdivieso, M.-H. (2006). The fission yeast Chs2 protein interacts with the type-II myosin Myo3p and is required for the integrity of the actomyosin ring. *J. Cell Sci.* **119**, 2768-2779.

Matsuyama, A., Yabana, N., Watanabe, Y. and Yamamoto, M. (2000). Schizosaccharomyces pombe Ste7p is required for both promotion and withholding of the entry to meiosis. *Genetics* **155**, 539-549.

Maupin, P. and Pollard, T. D. (1986). Arrangement of actin filaments and myosin-like filaments in the contractile ring and of actin-like filaments in the mitotic spindle of dividing HeLa cells. *J. Ultrastruct. Mol. Struct. Res.* **94**, 92-103.

Motegi, F., Nakano, K., Kitayama, C., Yamamoto, M. and Mabuchi, I. (1997). Identification of Myo3, a second type-II myosin heavy chain in the fission yeast Schizosaccharomyces pombe. *FEBS Lett.* **420**, 161-166.

Motegi, F., Nakano, K. and Mabuchi, I. (2000). Molecular mechanism of myosin-II assembly at the division site in Schizosaccharomyces pombe. *J. Cell Sci.* **113**, 1813-1825.

Motegi, F., Mishra, M., Balasubramanian, M. K. and Mabuchi, I. (2004). Myosin-II reorganization during mitosis is controlled temporally by its dephosphorylation and spatially by Mid1 in fission yeast. *J. Cell Biol.* **165**, 685-695.

Mukhina, S., Wang, Y.-L. and Murata-Hori, M. (2007). alpha-actinin is required for tightly regulated remodeling of the actin cortical network during cytokinesis. *Dev. Cell* **13**, 554-565.

Murphy, C. T., Rock, R. S. and Spudich, J. A. (2001). A myosin II mutation uncouples ATPase activity from motility and shortens step size. *Nat. Cell Biol.* **3**, 311-315.

Murthy, K. and Wadsworth, P. (2005). Myosin-II-dependent localization and dynamics of F-actin during cytokinesis. *Curr. Biol.* **15**, 724-731.

Nurse, P., Thuriaux, P. and Nasmyth, K. (1976). Genetic control of the cell division cycle in the fission yeast Schizosaccharomyces pombe. *Mol. Gen. Genet.* **146**, 167-178.

Patterson, B., Ruppel, K. M., Wu, Y. and Spudich, J. A. (1997). Cold-sensitive mutants G680V and G691C of Dictyostelium myosin II confer dramatically different biochemical defects. *J. Biol. Chem.* **272**, 27612-27617.

Pollard, T. D. (2010). Mechanics of cytokinesis in eukaryotes. *Curr. Opin. Cell Biol.* **22**, 50-56.

Reichl, E. M., Ren, Y., Morphew, M. K., Delannoy, M., Effler, J. C., Girard, K. D., Divi, S., Iglesias, P. A., Kuo, S. C. and Robinson, D. N. (2008). Interactions between myosin and actin crosslinkers control cytokinesis contractility dynamics and mechanics. *Curr. Biol.* **18**, 471-480.

Ruppel, K. M. and Spudich, J. A. (1996). Structure-function studies of the myosin motor domain: importance of the 50-kDa cleft. *Mol. Biol. Cell* **7**, 1123-1136.

Saha, S. and Pollard, T. D. (2012). Anillin-related protein Mid1p coordinates the assembly of the cytokinetic contractile ring in fission yeast. *Mol. Biol. Cell* **23**, 3982-3992.

Sanger, J. M. and Sanger, J. W. (1980). Banding and polarity of actin filaments in interphase and cleaving cells. *J. Cell Biol.* **86**, 568-575.

Shimada, T., Sasaki, N., Ohkura, R. and Sutoh, K. (1997). Alanine scanning mutagenesis of the switch I region in the ATPase site of Dictyostelium discoideum myosin II. *Biochemistry* **36**, 14037-14043.

Stachowiak, M. R., Laplante, C., Chin, H. F., Guirao, B., Karatekin, E., Pollard, T. D. and O'Shaughnessy, B. (2014). Mechanism of cytokinetic contractile ring constriction in fission yeast. *Dev. Cell* **29**, 547-561.

Stark, B. C., Sladewski, T. E., Pollard, L. W. and Lord, M. (2010). Tropomyosin and myosin-II cellular levels promote actomyosin ring assembly in fission yeast. *Mol. Biol. Cell* **21**, 989-1000.

Stark, B. C., James, M. L., Pollard, L. W., Sirotkin, V. and Lord, M. (2013). UCS protein Rng3p is essential for myosin-II motor activity during cytokinesis in fission yeast. *PLoS ONE* **8**, e79593.

Straight, A. F., Cheung, A., Limouze, J., Chen, I., Westwood, N. J., Sellers, J. R. and Mitchison, T. J. (2003). Dissecting temporal and spatial control of cytokinesis with a myosin II Inhibitor. *Science* **299**, 1743-1747.

Takaine, M., Numata, O. and Nakano, K. (2009). Fission yeast IQGAP arranges actin filaments into the cytokinetic contractile ring. *EMBO J.* **28**, 3117-3131.

Takaine, M., Numata, O. and Nakano, K. (2014a). Fission yeast IQGAP maintains F-actin-independent localization of myosin-II in the contractile ring. *Genes Cells* **19**, 161-176.

Takaine, M., Imada, K., Numata, O., Nakamura, T. and Nakano, K. (2014b). The meiosis-specific nuclear passenger protein is required for proper assembly of forespore membrane in fission yeast. *J. Cell Sci.* **127**, 4429-4442.

Uyeda, T. Q. P., Tokuraku, K., Kaseda, K., Webb, M. R. and Patterson, B. (2002). Evidence for a novel, strongly bound acto-S1 complex carrying ADP and phosphate stabilized in the G680V mutant of Dictyostelium myosin II. *Biochemistry* **41**, 9525-9534.

Uyeda, T. Q. P., Iwadate, Y., Umeki, N., Nagasaki, A. and Yumura, S. (2011). Stretching actin filaments within cells enhances their affinity for the myosin II motor domain. *PLoS ONE* **6**, e26200.

Vavylonis, D., Wu, J.-Q., Hao, S., O'Shaughnessy, B. and Pollard, T. D. (2008). Assembly mechanism of the contractile ring for cytokinesis by fission yeast. *Science* **319**, 97-100.

Wang, Y.-L. (2005). The mechanism of cortical ingression during early cytokinesis: thinking beyond the contractile ring hypothesis. *Trends Cell Biol.* **15**, 581-588.

Wilson, C. A., Tsuchida, M. A., Allen, G. M., Barnhart, E. L., Applegate, K. T., Yam, P. T., Ji, L., Keren, K., Danuser, G. and Theriot, J. A. (2010). Myosin II contributes to cell-scale actin network treadmilling through network disassembly. *Nature* **465**, 373-377.

Woods, A., Sherwin, T., Sasse, R., MacRae, T. H., Baines, A. J. and Gull, K. (1989). Definition of individual components within the cytoskeleton of Trypanosoma brucei by a library of monoclonal antibodies. *J. Cell Sci.* **93**, 491-500.

Wu, J.-Q. and Pollard, T. D. (2005). Counting cytokinesis proteins globally and locally in fission yeast. *Science* **310**, 310-314.

Wu, J.-Q., Kuhn, J. R., Kovar, D. R. and Pollard, T. D. (2003). Spatial and temporal pathway for assembly and constriction of the contractile ring in fission yeast cytokinesis. *Dev. Cell* **5**, 723-734.
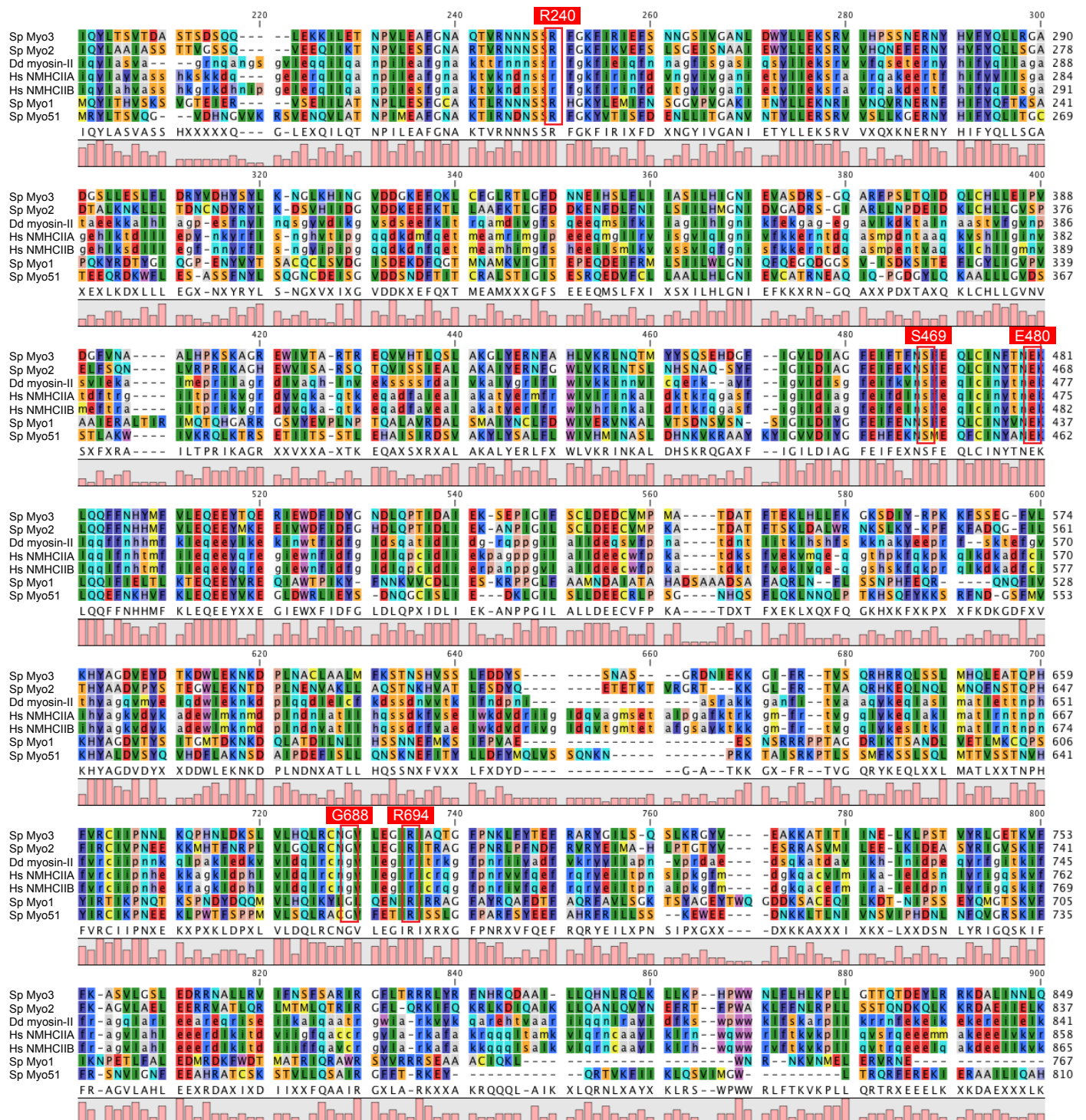
Fig. S1 Point-mutations introduced into Myo3

The deduced amino acid sequence of *S. pombe* Myo3 (Sp Myo3; GenBank accession no. AAC04615) was aligned with *S. pombe* Myo2 (Sp Myo2; AAC49908), the *D. discoideum* myosin-II heavy chain (Dd myosin-II; EAL64202), *H. sapiens* non-muscle myosin-IIA (MYH9) (Hs NMHCIIA; EAW60098), *H. sapiens* non-muscle myosin-IIB (MYH10) (Hs NMHCIIB; AAI17692), *S. pombe* Myo1 (type-I myosin) (Sp Myo1; CAB46766), and *S. pombe* Myo51 (type-V myosin) (Sp Myo51; CAA21172) by CLC Sequence Viewer 7. A part of the alignment (around residues 200-800) was shown. Boxed regions indicate conserved residues into which the mutations were introduced.
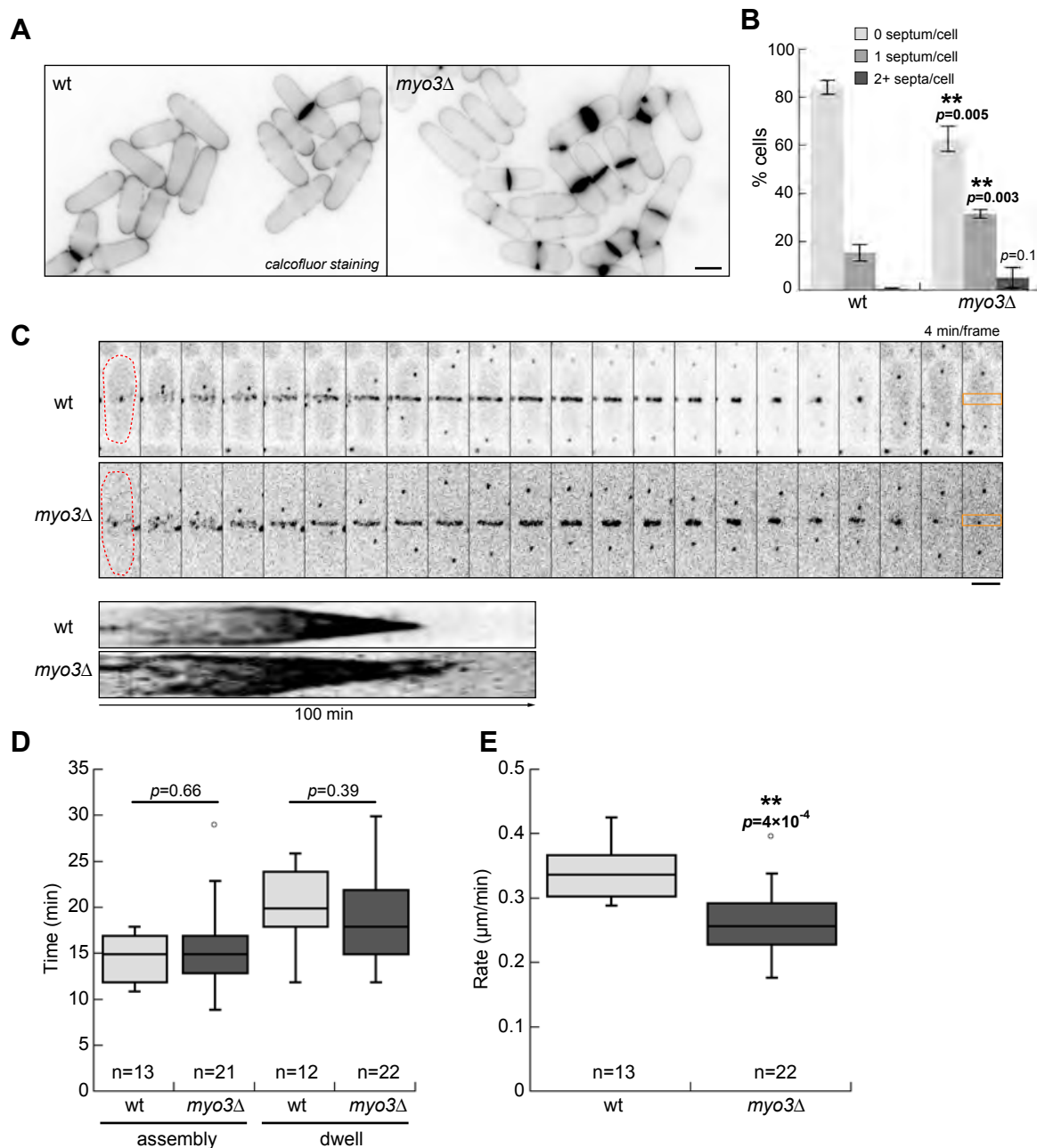
Fig. S2 Deletion of *myo3+* reduced the constriction rate of the CR and septation efficiency

(A) Septa of wt and *myo3Δ* cells grown at 30°C were stained and imaged. (B) Quantification of the number of septa per cell. Data are the mean ± SD (error bars) from three independent experiments (300-700 cells were scored at each measurement). (C) Time-lapse imaging of the assembly and constriction of Rlc1 rings in wt and *myo3Δ* cells. Bottom, kymographs of the boxed regions. (D) Box plots of the time required for the assembly of Rlc1 rings from the SPB separation and time of the dwell phase. (E) Box plot of the rate of Rlc1 ring constriction. Data in (D-E) were pooled from two independent experiments. Double asterisks indicate a significant difference (p < 0.01). Bars, 5 μm.
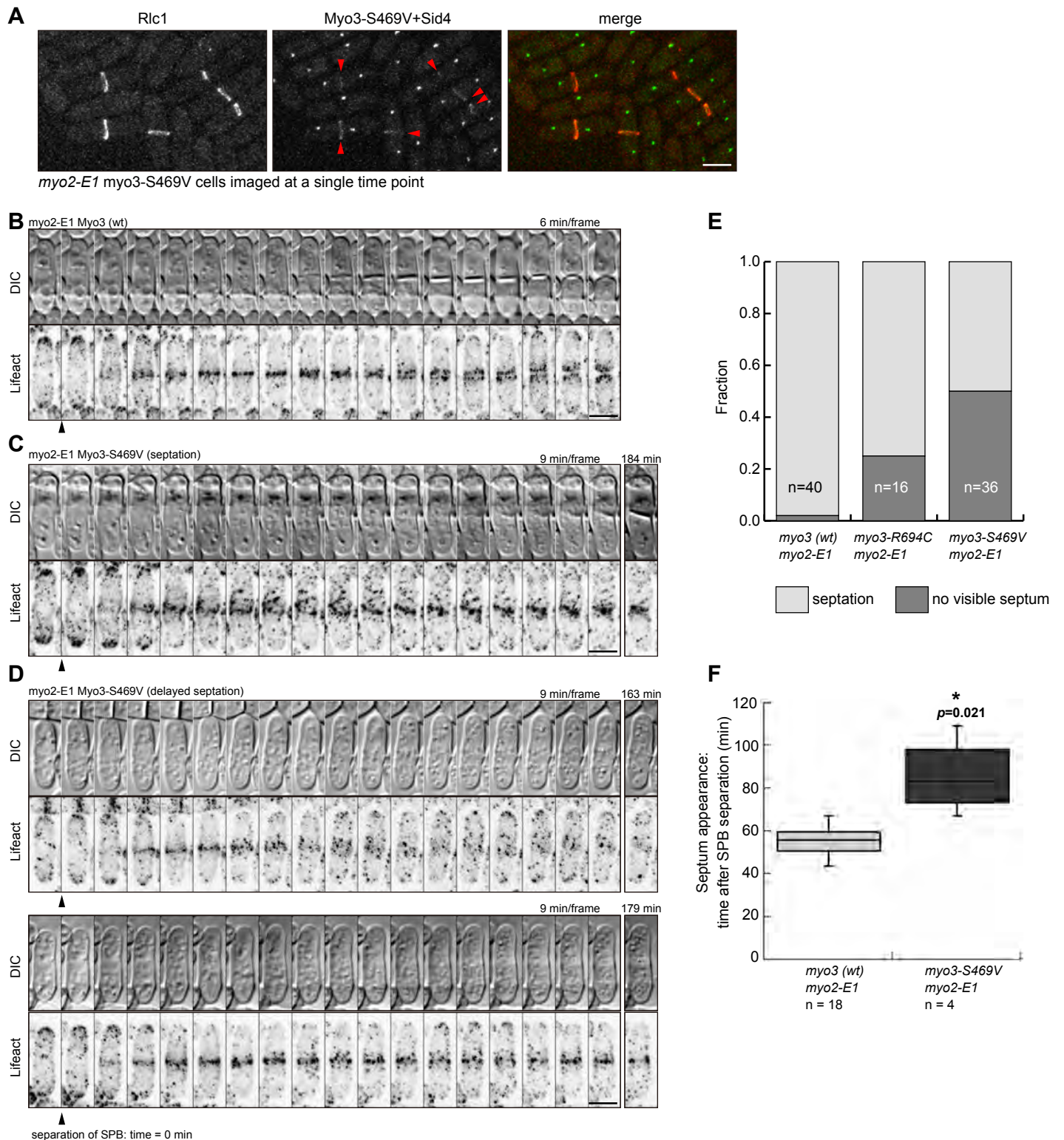
Fig. S3 Behavior of the medial actin ring in *myo2-E1* myo3-S469V cells

(A) A stack of z-sections of *myo2-E1* rlc1-3mCherry myo3-S469V-3mYFP sid4-3mYFP cells was acquired at a single time point using a confocal microscope (LSM 700; Carl Zeiss, Inc.). The experimental conditions were the same as those used in Figure 5, except that cells were not repeatedly scanned by lasers. Arrowheads indicate Myo3-S469V-3mYFP localizing to the CR in the *myo2-E1* background. (B-D) Observation of the medial actin ring during cytokinesis in cells expressing Myo3-3mYFP (B) or Myo3-S469V (C, D) in the *myo2-E1* background. Arrowheads indicate the timing of the SPB separation. (E) The cells of the indicated genotypes were scored according to septum formation in bright field images. These cells were observed for at least 70 (wt) or 95 (R694C and S469V) min after the SPB separation. (F) Box plot of the time from SPB separation to the appearance of a visible septum. An asterisk indicates a significant difference (vs. wt, p < 0.05). Data in (E-F) were pooled from two independent experiments. Bars, 5 μm.
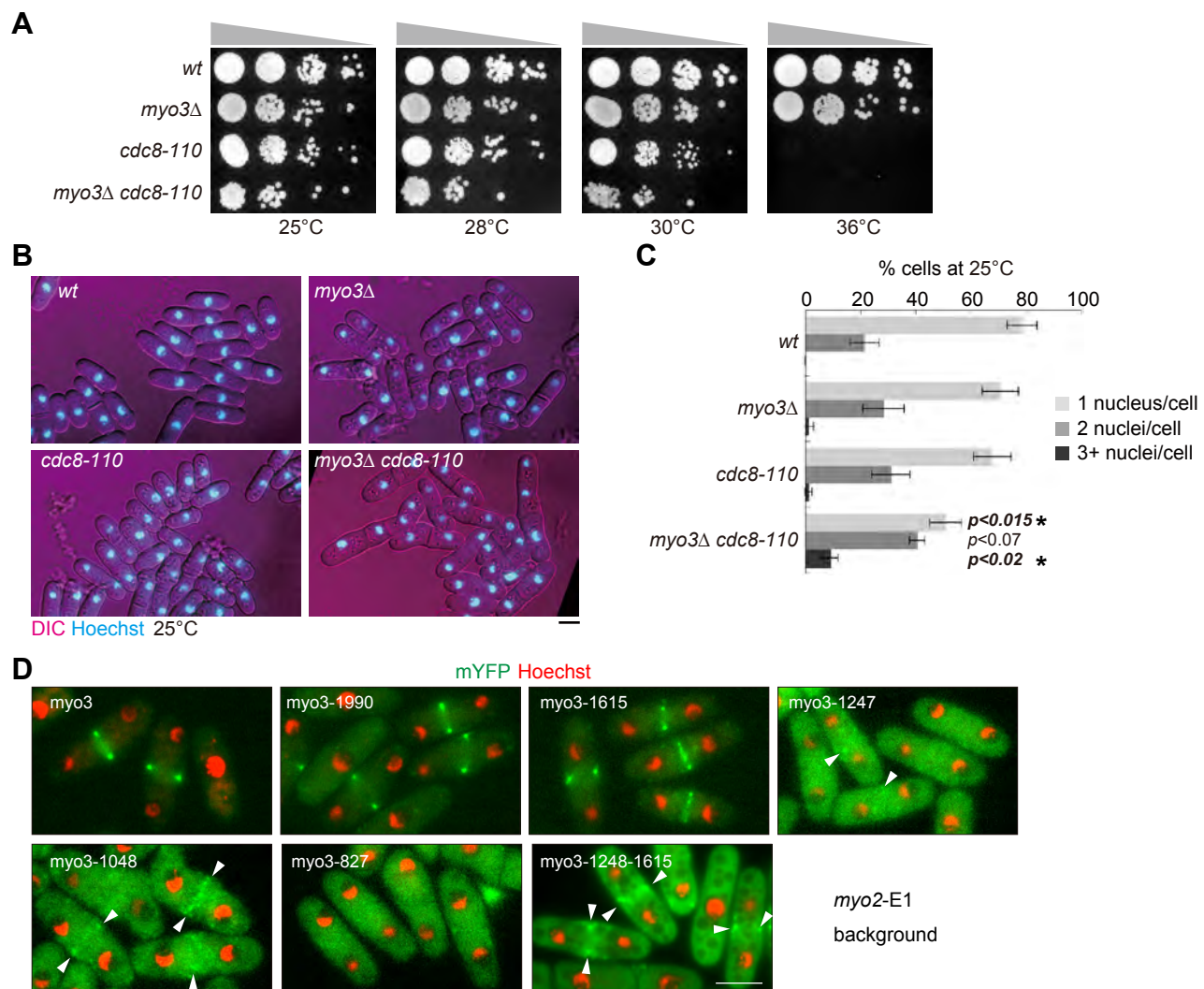
A

B

DIC Hoechst 25°C

C

% cells at 25°C

1 nucleus/cell
2 nuclei/cell
3+ nuclei/cell

p<0.015 *
p<0.07
p<0.02 *

D

mYFP Hoechst

myo2-E1 background

Fig. S4 Genetic interaction between *myo3Δ* and *cdc8-110*, and localization of the myo3 deletion forms in the *myo2*-E1 background

(A) Cells of the indicated genotypes were serially diluted, spotted on plates, and grown for 3 days at the indicated temperature. (B) Cells were grown at 25°C, stained with Hoechst, and then imaged in a single focal plane. (C) Quantification of the number of nuclei per cell. Data are the mean ± SD (error bars) from three independent experiments (250-500 cells were scored at each measurement). P-values were calculated versus the three other strains, and the most stringent conditions were shown. Asterisks indicate a significant difference (p < 0.05). (D) Localization of the myo3 deletion forms in the *myo2*-E1 background. Cells expressing the indicated forms of Myo3-3mYFP were imaged in a single focal plane. Myo3-1245-1615-3mYFP was expressed under the control of the nmt41 promoter in the absence of thiamine for 36 h. Arrowheads indicate the medial localization of mutant myo3s. Bars, 5 μm.

Table S1. Strains used in this study

Name	Genotype	Source	Figure
MTY672	myo3Δhead::ura4 (delete 0.4-2.4kbp)-3mYFP-3HA:hphMX6	This study	
MTY616	mYFP-Myo2 Pcdc4-lifeact-4mCherry sid4-3mYFP-3HA:hph	Lab stock	1
MTY597	myo3-3mYFP-3HA:hph sid4-3mYFP-3HA:kan Pcdc4-lifeact-4mCherry	This study	1, 2
MTY904	mid1Δ::ura4 myo3-3mYFP-3HA:hph sid4-3mYFP-3HA:kan Pcdc4-lifeact-4mCherry	This study	2
MTY1020	myo3-G688V-3mYFP-3HA-hphMX6 sid4-4mCherry:kanMX6	This study	3
MTY465	myo3-3mYFP-3HA:hphMX6	This study	3
MTY473	myo3-S469V-3mYFP-3HA:hphMX6	This study	3
MTY474	myo3-R694C-3mYFP-3HA:hphMX6	This study	3
MTY497	myo3-E480K-3mYFP-3HA:hphMX6	This study	3
MTY498	myo3-R240A-3mYFP-3HA:hphMX6	This study	3
MTY642	kan:Pnmt41-myo3-3mYFP-3HA:hph	This study	3
MTY685	myo3-G688V-3mYFP-3HA:hphMX6	This study	3
MTY693	myo3-G688V-3mYFP-3HA rlc1-3mCherry sid4-3mYFP-3HA	This study	3
MTY716	myo3-E480K-3mYFP-3HA sid4-3mYFP-3HA	This study	3
MTY718	myo3-R240A-3mYFP-3HA sid4-3mYFP-3HA:kan	This study	3
MTY719	myo3-G688V-3mYFP-3HA sid4-3mYFP-3HA	This study	3
MTY724	myo3-S469V-3mYFP-3HA sid4-3mYFP-3HA:kan	This study	3
MTY528	myo3-3mYFP-3HA:hphMX6 sid4-3mYFP-3HA:kan	This study	3, 7
MTY569	kan:Pnmt41-myo3tail-3mYFP-3HA:hphMX6	This study	3, 7
MTY717	myo3-R694C-3mYFP-3HA sid4-3mYFP-3HA:kan	This study	3, 7
MTY551	myo3-3mYFP-3HA:hphMX6 rlc1-3mCherry sid4-3mYFP-3HA	This study	4
MTY704	myo3-S469V-3mYFP-3HA rlc1-3mCherry sid4-3mYFP-3HA	This study	4
MTY913	myo3-R694C-3mYFP-3HA rlc1-3mCherry sid4-3mYFP-3HA	This study	4
MTY636	rlc1-3mYFP-3HA sid4-3mYFP-3HA:kan	Lab stock	6, S2
MTY684	myo3Δ:kan rlc1-3mYFP-3HA sid4-3mYFP-3HA:kan	This study	6, S2
MTY777	myo2-E1 myo3-3mYFP-3HA rlc1-3mCherry sid4-3mYFP-3HA	This study	4, 5
MTY778	myo2-E1 myo3-R694C-3mYFP-3HA rlc1-3mCherry sid4-3mYFP-3HA	This study	4, 5
MTY780	myo2-E1 myo3-S469V-3mYFP-3HA rlc1-3mCherry sid4-3mYFP-3HA	This study	4, 5, S3
MTY982	cdc8-110 rlc1-3mYFP-hphMX6 sid4-3mYFP-3HA	This study	6
MTY983	cdc8-110 myo3Δ::kan rlc1-3mYFP-hphMX6 sid4-3mYFP-3HA	This study	6

MTY1001	myo3-1990-3mYFP-3HA:hphMX6	This study	7
MTY1002	myo3-1615-3mYFP-3HA:hphMX6	This study	7
MTY1003	myo3-1247-3mYFP-3HA:hphMX6	This study	7
MTY1004	myo3-827-3mYFP-3HA:hphMX6	This study	7
MTY1008	myo3-1048-3mYFP-3HA:hphMX6	This study	7
MTY1010	kanMX6:Pnmt41-myo3-1248-1615-3mYFP:hphMX6	This study	7
MTY838	myo2-E1 myo3-3mYFP-3HA:hph sid4-3mYFP-3HA:kan Pcdc4-lifeact-4mCherry	This study	S3
MTY839	myo2-E1 myo3-S469V-3mYFP-3HA sid4-3mYFP-3HA Pcdc4-lifeact-4mCherry:ura4	This study	S3
MTY840	myo2-E1 myo3-R694C-3mYFP-3HA sid4-3mYFP-3HA Pcdc4-lifeact-4mCherry:ura4	This study	S3
MTY10	ura4D-18 leu1-32	Lab stock	S4
MTY16	cdc8-110	Lab stock	S4
MTY78	myo3Δ::kanMX6	This study	S4
MTY88	myo3Δ::kanMX6 cdc8-110	This study	S4
MTY1078	myo2-E1 myo3-3mYFP-3HA:hphMX6	This study	S4
MTY1079	myo2-E1 myo3-1990-3mYFP-3HA:hphMX6	This study	S4
MTY1080	myo2-E1 myo3-1615-3mYFP-3HA:hphMX6	This study	S4
MTY1081	myo2-E1 myo3-1247-3mYFP-3HA:hphMX6	This study	S4
MTY1082	myo2-E1 myo3-1048-3mYFP-3HA:hphMX6	This study	S4
MTY1083	myo2-E1 myo3-827-3mYFP-3HA:hphMX6	This study	S4
MTY1084	myo2-E1 kanMX6:Pnmt41-myo3-1248-1615-3mYFP:hphMX6	This study	S4

Table S2. Plasmids used in this study

Name	Structure	Source	Purpose
MTP467	pREP81-GFP-myo3	Lab stock	
MTP461	pREP81-GFP-myo3-R240A	This study	MTY498
MTP465	pREP81-GFP-myo3-G688V	This study	MTY685
MTP466	pREP81-GFP-myo3-E480K	This study	MTY497
MTP486	pREP81-GFP-myo3-S469V	This study	MTY473
MTP487	pREP81-GFP-myo3-R694C	This study	MTY474

Movies
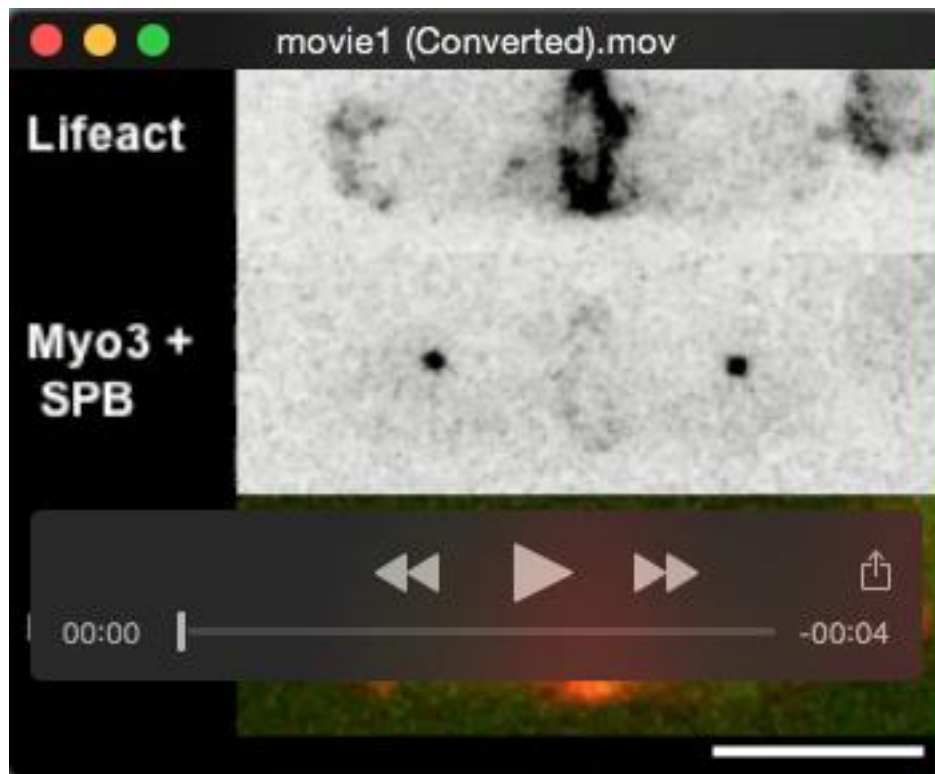
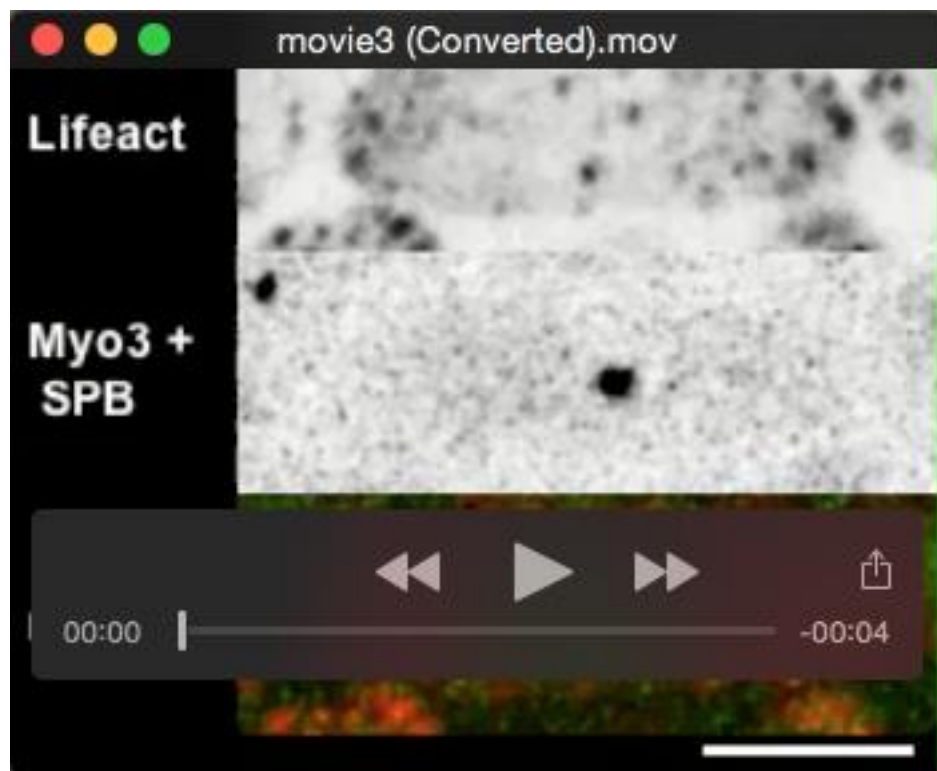**Movie 1. Myo3 and actin rings in DMSO-treated cells.** Related to Figure 1C. Strain:

MTY597 (*myo3-3mYFP sid4-3mYFP Pcdc4-lifeact-4mCherry*). Time-lapse imaging of

Myo3-3mYFP and actin rings using an inverted fluorescence microscope (BX71; Olympus)

equipped with a UPlanSApo 100×/1.40 NA objective lens (Olympus), spinning-disk confocal

scanner (CSU22; Yokogawa), piezo objective positioner (E-665; Physik Instrumente),

electron multiplying CCD camera (iXon 3 885; Andor), and emission beam splitter (Dual

View; Roper Scientific) with excitation by 488-nm and 568-nm lasers using GFP and

mCherry filters and MetaMorph software (version 7.7.5.0; Molecular Devices). Myo3,

Lifeact, and SPBs in late anaphase cells were simultaneously imaged at 1-min intervals. A

total of 0.36% DMSO was supplemented at t = 00:00. Stacks of 12 confocal *z*-sections spaced

by 0.45 µm were collected every minute for 30 min, and projected to an *xy* image using a

maximum intensity projection. Green, Myo3-3mYFP and Sid4-3mYFP; red, Lifeact-

4mCherry. Bar, 5 µm.

Movie 2. Myo3 and actin rings in Lat-A-treated cells. Related to Figure 1D. Strain: MTY597 (*myo3-3mYFP sid4-3mYFP Pcdc4-lifeact-4mCherry*). Time-lapse imaging of Myo3-3mYFP and actin rings using an inverted fluorescence microscope (BX71; Olympus) equipped with a UPlanSApo 100×/1.40 NA objective lens (Olympus), spinning-disk confocal scanner (CSU22; Yokogawa), piezo objective positioner (E-665; Physik Instrumente), electron multiplying CCD camera (iXon 3 885; Andor), and emission beam splitter (Dual View; Roper Scientific) with excitation by 488-nm and 568-nm lasers using GFP and mCherry filters and MetaMorph software (version 7.7.5.0; Molecular Devices). Myo3, Lifeact, and SPBs in late anaphase cells were simultaneously imaged at 1-min intervals. A total of 0.36% DMSO plus 7 µM Lat-A was supplemented at t = 00:00. Stacks of 12 confocal *z*-sections spaced by 0.45 µm were collected every minute for 30 min, and projected to an *xy* image using a maximum intensity projection. Green, Myo3-3mYFP and Sid4-3mYFP; red, Lifeact-4mCherry. Bar, 5 µm.

Movie 3. Assembly of Myo3 and actin rings. Related to Figure 2A. Strain: MTY597 (*myo3-3mYFP sid4-3mYFP Pcdc4-lifeact-4mCherry*). Time-lapse imaging of Myo3-3mYFP and actin rings using a confocal microscope (LSM 700; Carl Zeiss, Inc.) equipped with an alpha Plan-Apochromat 100×/1.46 NA objective lens (Carl Zeiss, Inc.). The duplicated SPBs separated at t = 00:00. Stacks of 12 confocal *z*-sections spaced by 0.62 μm were collected every 2 minutes for 60 min, and projected to an *xy* image using a maximum intensity projection. Green, Myo3-3mYFP and Sid4-3mYFP; red, Lifeact-4mCherry. Bar, 5 μm.

Movie 4. Assembly of Myo3 and Rlc1 rings. Related to Figures 4A-B. Strains: MTY551 (*myo3-3mYFP rlc1-3mCherry sid4-3mYFP*) (*left* column) and MTY913 (*myo3-R694C-3mYFP rlc1-3mCherry sid4-3mYFP*) (*right* column). Time-lapse imaging of Myo3 and Rlc1 rings using a confocal microscope (LSM 700; Carl Zeiss, Inc.) equipped with an alpha Plan-Apochromat 100×/1.46 NA objective lens (Carl Zeiss, Inc.). The duplicated SPBs separated at t = 00:00. Stacks of 13 confocal *z*-sections spaced by 0.62 µm were collected every 2 minutes for 90 min, and projected to an *xy* image using a maximum intensity projection. Green, Myo3-3mYFP and Sid4-3mYFP; red, Rlc1-3mCherry. Bar, 5 µm.
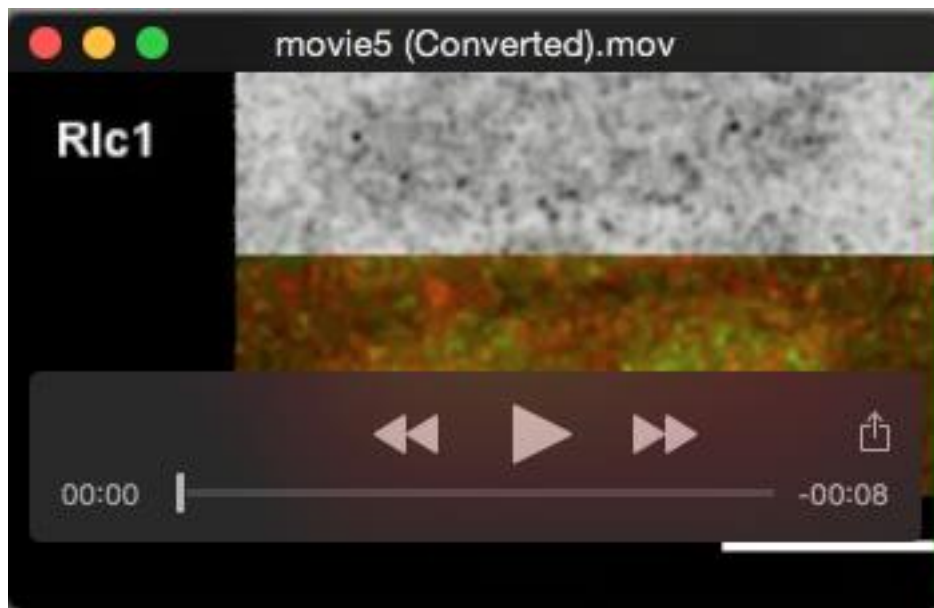
Movie 5. Constriction of the Rlc1 ring in the *myo2-E1 myo3-S469V* background. Related to the upper panel of Figure 5C. Strain: MTY780 (*myo2-E1 myo3-S469V-3mYFP rlc1-3mCherry sid4-3mYFP*). Time-lapse imaging of Myo3-S469V and Rlc1 rings using a confocal microscope (LSM 700; Carl Zeiss, Inc.) equipped with an alpha Plan-Apochromat 100×/1.46 NA objective lens (Carl Zeiss, Inc.). The duplicated SPBs separated at t = 00:00. Stacks of 13 confocal *z*-sections spaced by 0.62 µm were collected every 3 minutes for 180 min, and projected to an *xy* image using a maximum intensity projection. Green, Myo3-S469V-3mYFP and Sid4-3mYFP; red, Rlc1-3mCherry. Bar, 5 µm.

Movie 6. Collapse of the Rlc1 ring in the *myo2-E1 myo3-S469V* background. Related to the middle and bottom panels of Figure 5C. Strain: MTY780 (*myo2-E1 myo3-S469V-3mYFP rlc1-3mCherry sid4-3mYFP*). Time-lapse imaging of Myo3-S469V and Rlc1 rings using a confocal microscope (LSM 700; Carl Zeiss, Inc.) equipped with an alpha Plan-Apochromat 100×/1.46 NA objective lens (Carl Zeiss, Inc.). Left and right columns correspond to the middle and bottom panels shown in Figure 5C, respectively. Stacks of 13 confocal *z*-sections spaced by 0.62 µm were collected every 3 minutes for 180 min, and projected to an *xy* image using a maximum intensity projection. Green, Myo3-S469V-3mYFP and Sid4-3mYFP; red, Rlc1-3mCherry. Bar, 5 µm.

Movie 7. Behavior of Rlc1 rings in *myo3Δ cdc8-110* cells. Related to Figure 6B. Strain: MTY983 (*cdc8-110 myo3Δ rlc1-3mYFP sid4-3mYFP*). Time-lapse imaging of the Rlc1 ring and SPBs using an inverted fluorescence microscope (BX71; Olympus) equipped with a UPlanSApo 100×/1.40 NA objective lens (Olympus), a spinning-disk confocal scanner (CSU22; Yokogawa), piezo objective positioner (E-665; Physik Instrumente), and electron multiplying CCD camera (iXon 3 885; Andor) with excitation by a 488-nm laser using a GFP filter and MetaMorph software (version 7.7.5.0; Molecular Devices). An asterisk indicates the cell shown in the bottom panel of Figure 6B. Stacks of 13 confocal *z*-sections spaced by 0.60 μm were collected every 2 minutes for 240 min, and projected to an *xy* image using a maximum intensity projection. Bar, 5 μm.
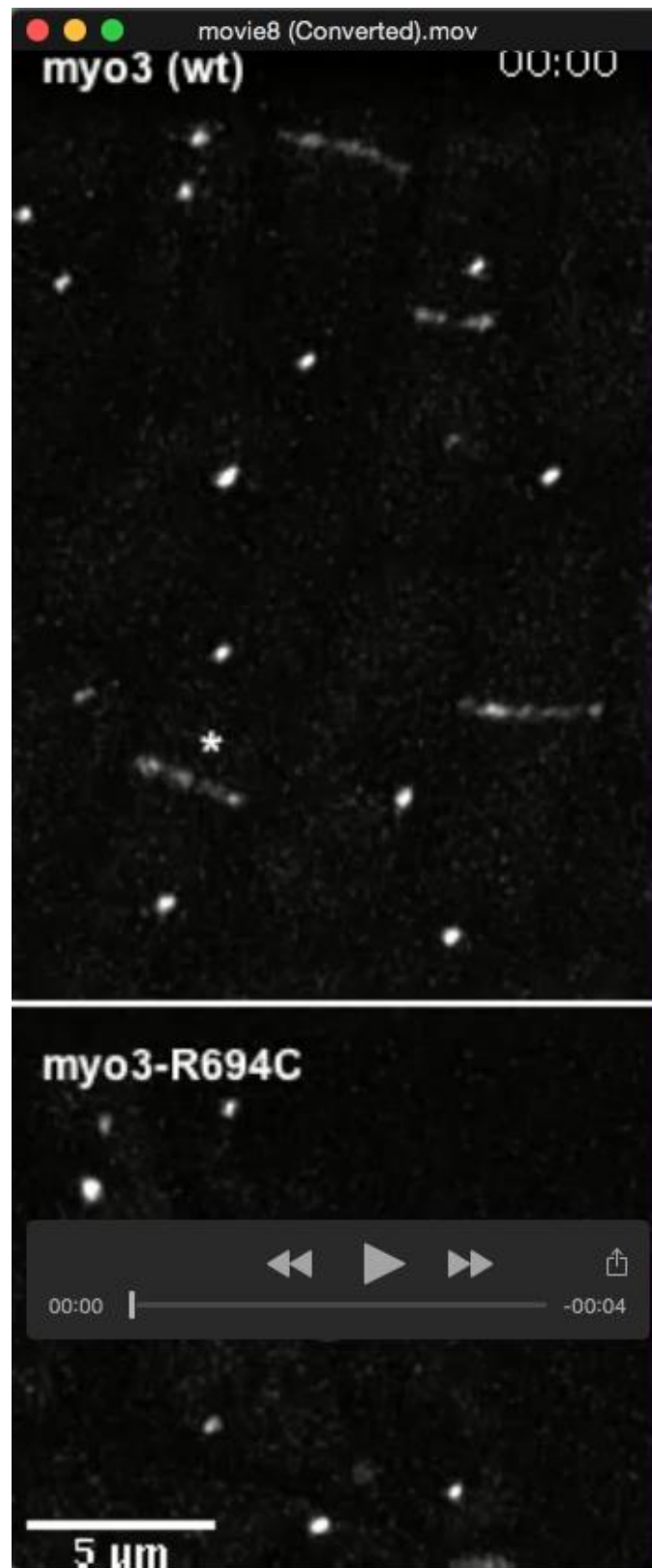
Movie 8. Motile Myo3 clusters on the contractile ring. Related to Figure 7D. Strains:

MTY528 (*myo3-3mYFP sid4-3mYFP*) and MTY717 (*myo3-R694C-3mYFP sid4-3mYFP*).

Time-lapse imaging of the Myo3 ring and SPBs using an inverted fluorescence microscope (BX71; Olympus) equipped with a UPlanSApo 100×/1.40 NA objective lens (Olympus), spinning-disk confocal scanner (CSU22; Yokogawa), piezo objective positioner (E-665; Physik Instrumente), and electron multiplying CCD camera (iXon 3 885; Andor) with excitation by a 488-nm laser using a GFP filter and MetaMorph software (version 7.7.5.0; Molecular Devices). Asterisks indicate the cells shown in Figure 7D (the bottom panel for wt). Stacks of 9 confocal *z*-sections spaced by 0.31 μm (corresponding to the lower half of the contractile ring) were collected every 15 s for 8 min. The stacked images were deconvolved using Huygens Essential software (version 4.5; Scientific Volume Imaging) based on the classic maximum likelihood estimation method, and projected to an *xy* image using a maximum intensity projection. Bar, 5 μm.